Diploma Thesis

Clinical Acceptable Image Noise in Pediatric Computed Tomography Examinations— A Retrospective Analysis

Submitted by
Karla Rodriguez Dominguez

For the acquisition of the academical grade

Doktor(in) der gesamten Heilkunde
(Dr. med. univ.)

at the
Medical University Graz

conducted at the
Department of Radiology, Division of Pediatric Radiology

under the guidance of head supervisor
UnivProf. DDr.hc Erich Sorantin
and joint supervisor
Dr. med. Eszter Nagy

Graz, am 23.03.2020

EIDESSTATTLICHE ERKLÄRUNG

Ich erkläre ehrenwörtlich, dass ich die vorliegende Arbeit selbstständig und ohne fremde Hilfe verfasst habe, andere als die angegebenen Quellen nicht verwendet habe und die den benutzten Quellen wörtlich oder inhaltlich entnommenen Stellen als solche kenntlich gemacht habe.

Graz, am 23.03.2020 *Karla Rodriguez Dominguez eh.*

AKNOWLEDGEMENTS

First and foremost, I would like to extend my immense gratitude towards Univ.-Prof. Dr. Erich Sorantin. After all, this study would have not been possible without his innovative idea and his years of experience in the radiological field. Special thanks to Dr. Eszter Nagy, who guided me throughout this project and helped me with endless patience

Many thanks to the pediatric radiology department team in the University Hospital Graz for facilitating the recollection of the data and the measurements made. To Dr. Sebastian Tschauner and to the whole team who gladly gave me advice during this strenuous work.

To my friends and family always keeping my spirits high, who believed in me and encouraged me to keep going. Particularly to Andrea, Carlos and my sister Pamela, proofreading is no funny task, but you still went out of the way for me. To my beloved husband Bernhard, many thanks for the unconditional support.

Lastly, special thanks to my parents Guillermo and Malena. There are no words to express how grateful I am for your eternal support. This work is dedicated to you.

TABLE OF CONTENTS

EIDESSTATTLICHE ERKLÄRUNG 2

AKNOWLEDGEMENTS 3

ABBREVIATIONS 6

ABSTRACT 7

INTRODUCTION 7
MATERIALS AND METHODS 7
RESULTS 7
CONCLUSION 7

ZUSAMMENFASSUNG 8

EINLEITUNG 8
MATERIALEN UND METHODEN 8
ERGEBNISSE 8
FAZIT 9

INTRODUCTION 10

TRENDS IN RADIOLOGICAL EXPOSURE 12
IMAGE QUALITY 13
DIAGNOSTIC REQUIREMENTS *14*
PHYSICAL AND TECHNICAL PARAMETERS WITH IMPACT ON IMAGE QUALITY *14*
Noise 14
Slice Thickness 14
Exposure Factors 15
ESTIMATIONS OF RADIATION DOSE 15
EFFECTIVE DOSE *15*
CT DOSE INDEX (CTDI) *16*
DLP (DOSE-LENGTH PRODUCT) *16*
EFFECTIVE DIAMETER AND SSDE (SIZE-SPECIFIC DOSE ESTIMATE) *16*
RADIATION DOSE RISKS 17
THEORIES ON RADIATION EFFECTS *17*
RADIATION-INDUCED CANCER *18*
CT RADIATION EXPOSURE: THE PEDIATRIC ISSUE *19*
RADIATION DOSE OPTIMIZATION ATTEMPTS 20

MATERIALS AND METHODS 22

STUDY SETTING 22
SAMPLE 22
ANONYMIZATION 23
MEASURES AND PROCEDURES 23
SUBJECTIVE EVALUATION 27
STATISTICAL ANALYSIS 32
OBJECTIVE DATA ANALYSIS *32*
SUBJECTIVE DATA ANALYSIS *32*

RESULTS 33

BASELINE DATA 33
IMAGE NOISE ANALYSIS 42
HEAD EXAMINATIONS *42*
CHEST EXAMINATIONS *44*
ABDOMINAL EXAMINATIONS *47*
SUBJECTIVE DATA ANALYSIS 50
NATIVE HEAD EXAMINATIONS *51*
HEAD EXAMINATIONS WITH CM *52*
NATIVE CHEST EXAMINATIONS *53*
CHEST EXAMINATIONS WITH CM *54*
NATIVE ABDOMINAL EXAMINATIONS *56*

ABDOMINAL EXAMINATIONS WITH CM *57*

DISCUSSION **59**

LIMITATIONS 61
CONCLUSION 61

REFERENCES **62**

ABBREVIATIONS

3D	three dimensions
ALARA	as low as reasonably achievable
AAPM	American Association of Physicists in Medicine
AP	anteroposterior
CI	confidence interval
CT	computed tomography
CTDI	computed tomography dose index
DRL	diagnostic reference levels
DLP	dose length product
EMI	Electric and Musical Industries
Fig.	figure
Gy	Gray
HU	Hounsfield units
IR	iterative reconstruction
kV	kilovolt
LNT	linear no-threshold theory
mA	milliamperes
mAs	milliamperes per second
MDCT	multidetector computed tomography
mGy	microGrays
MSCT	multislice computer tomography
PACS	picture archiving and communication system
ROI	region of interest
SD	standard deviation
SE	standard error
SSCT	single slice computer tomography
SSDE	size-specific dose estimate
UK	United Kingdom
USA	United States of America

ABSTRACT

INTRODUCTION

The use of plain radiographies and CTs comes with an unavoidable radiation exposure. CT examinations in pediatric patients represent one of the highest challenges to radiologists because of their higher sensitivity to radiation's harmful side effects. This study aims to obtain noise measurements in diagnostic CT scans to define clinically acceptable noise.

MATERIALS AND METHODS

A database of 620 CT examinations was retrieved at the Radiology Department, Division of Pediatric Radiology at University Hospital Graz. Data was anonymized. Image noise, as well as other key technical parameters, was retrieved from the images. Image noise was measured in head, chest and abdomen CT scans. Results were analyzed descriptively as well as with statistical tests. Subjective image analysis was performed according to two grading scales and analyzed descriptively.

RESULTS

In native head CTs, image noise in centrum semiovale was significantly lower at 100 kV than at 80 kV and 120 kV tube voltages ($p<0,05$). Significantly higher image noise was seen in the aortic arch with 100 kV than with 120 kV. Enhanced head and chest examinations with 100 kV presented significantly higher image noise than the native ones. Measurements in native abdominal examinations with 100 kV showed significantly higher image noise ($p=0,012$) when compared to those with 120 kV. No significant difference was seen between native and CM examinations.

Subjective evaluation of native head examinations revealed minimal image noise in 61% of the cases as well as optimal image quality in 92% of the cases. 64% of native chest examinations was scored with "moderate" image noise, the subjective image quality was "acceptable" in 88% of the cases was. 77% of the enhanced chest examinations were "acceptable", 56% had "moderate" image noise. 67% of the enhanced abdominal examinations had "moderate" image noise, and 84% were "acceptable".

CONCLUSION

Establishing clinical acceptable image noise ranges within different anatomical regions may contribute in the development of CT protocols to provide the best possible diagnostic information at the lowest possible dose.

ZUSAMMENFASSUNG

EINLEITUNG

Die Verwendung von konventionellen Röntgenaufnahmen und CTs ist mit einer unvermeidbaren Strahlenexposition verbunden. Pädiatrische CT stellt eine große Herausforderung für Radiologen dar, da sie empfindlicher auf die schädlichen Nebenwirkungen der Strahlung sind. Um die Strahlenbelastung zu minimieren und die diagnostische Wertigkeit beizubehalten, ist eine kontinuierliche Entwicklung der CT Protokolle empfehlenswert. Diese Studie zielt auf Geräuschmessungen in diagnostischen CT-Scans ab, damit ein klinisch akzeptables Bildrauschen in der Zukunft definiert werden kann.

METHODEN

Eine anonymisierte Datenbank mit 620 CT-Untersuchungen wurde an der Klinischen Abteilung für Kinderradiologie des Universitätsklinikums Graz abgerufen. Bildrauschen sowie wichtige technische Parameter wurden aus CT des Gehirnschädels, Thorax und Abdomen in bestimmten Regionen erhoben. Die gemessenen Ergebnisse wurden deskriptiv und mit statistischen Tests analysiert. Die subjektive Bildanalyse wurde nach zwei Bewertungsskalen durchgeführt und deskriptiv analysiert.

ERGEBNISSE

Das Bildrauschen in nativen CT des Gehirnschädels war signifikant weniger bei 100 kV als bei 80 kV oder 120 kV ($p < 0,05$). Das Bildrauschen bei 100 kV in kontrastmittelunterstützten CT-Gehirnschädel und CT-Thorax war signifikant höher als ohne Kontrastmittel. In nativen Thoraxuntersuchungen mit 100 kV wurde ein signifikant höheres Bildrauschen beobachtet als mit 120 kV. Messungen bei nativen Abdomenuntersuchungen mit 100 kV zeigten ein signifikant höheres Bildrauschen ($p = 0,012$) im Vergleich zu Messungen mit 120 kV. Es wurde kein signifikanter Unterschied zwischen nativen und kontrastmittelunterstützten CT-Abdomen festgestellt.

Die subjektive Analyse des Bildrauschens in nativen CT des Gehirnschädels ergab ein „minimales“ Bildrauschen in 61% der Fälle bzw. eine „optimale“ subjektive Bildqualität in 92% der Fälle. Bei den nativen Thoraxuntersuchungen 64% wurde mit „mäßigem“ Bildrauschen und 88% als „akzeptabel“ bewertet. 77% der Thoraxuntersuchungen mit Kontrastmittel waren "akzeptabel" und 56% hatten „mäßiges“ Bildrauschen. 67% der

Abdomenuntersuchungen mit Kontrastmittel wiesen ebenfalls ein „mäßiges“ Bildrauschen auf und 84% waren „akzeptabel“.

FAZIT

Die Festlegung klinisch akzeptabler Bereiche des Bildrauschens in verschiedenen anatomischen Regionen kann in der Zukunft zur Entwicklung von CT-Protokollen beitragen, welche eine optimale Diagnose bei möglichst geringer Dosis gewährleisten.

INTRODUCTION

Diagnostic imaging is a crucial tool for medical physicians to make a faster and more accurate diagnosis. Radiological imaging has come a long way since the first-ever made radiography into today's contrast-aided computed tomography (CT). However, the use of plain radiographies and CTs comes with an unavoidable radiation exposure, which can be potentially harmful not only to patients but also to health personnel. Imaging techniques and protocols have evolved to gain the most diagnostic information with the least radiation possible. Numerous research studies have been performed on this topic in adults[3–8], as well as in children[9–13].

Pediatric patients represent one of the biggest challenges to radiologists. On the one hand, not only do children have different anatomical and physiological features, which change rapidly within years or even months, but also, they are more sensitive to radiation. On the other hand, the youngest children are not able to follow instructions during the image acquisition. These factors make it a necessity to adjust imaging protocols to pediatric patients and their most commonly presented diseases to maintain diagnostic accuracy.

In an effort to minimize radiation exposure but at the same time maintain an acceptable image quality, scanning protocols concerning specific radiation dosage have been developed. European and national diagnostic dose reference levels for children were last updated in 2016[1, 2]. However, image quality is not only affected by radiation dose, but also other parameters. Image noise is often explored in the literature but not a part of scanning protocols.

This study aims to obtain data of a clinically acceptable noise to help define image noise ranges. By analyzing the different technical factors that constitute image quality, the lead researcher intends to focus on image noise as well as the different technical factors that influence it. Technical aspects of CT, as well as the special considerations in the pediatric population, are explained in more detail to provide a more comprehensive overview of the subject.

HISTORICAL BACKGROUND OF CT

German physicist Wilhelm Conrad Röntgen is worldwide known for the discovery of X-rays. In 1895[14], this meant a gigantic milestone reached by medicine and the beginning of imaging diagnostic as a medical field. Nonetheless, its development kept on going at a steady

pace, with some concepts already hinting at how it would come to be an essential item in today's medical diagnosis.

Research as early as 1905 from Dutch physicist H.A. Lorentz and 1917 from mathematician J.H. Radon created a precedent for the development of CT scanners. In the late fifties, oblivious to his predecessors, physicist A.M. Cormack led one of the first experiments with reconstructive imaging in the medical field. He was able to develop a method based on transmission measurements, which could calculate radiation absorption distributions in the human body [15]. However, it was English engineer G.N. Hounsfield who made a practical implementation of the previous theories and is now recognized as the father of Computer Tomography. It was in 1972 when he, backed up by British firm EMI Ltd, successfully conducted the first clinical examinations with the first-ever built CT machine.[15]

CT scan posed a very particular superiority to plain radiographies. "The system is approximately 100 times more sensitive than conventional X-ray systems to such an extent that variations in soft tissues of nearly similar density can be displayed" [16]. As expected, its development afterwards was highly encouraged, and just two years after its invention, EMI lost the exclusive rights over its patent and production [17]. Other CT manufacturers began to get involved in the further development of the CT machine. Increasing the speed in which scanners acquired images became a growing need in its development, and between 1980 to 1990 manufacturers were able to reduce scan time 1 to 2 seconds.[17]

The term "tomography" was coined after the Greek words *tomos* (slice) and *graphein* (draw)[18]. Furthermore, the word "computer" was added to describe the digitalization part of the imaging process. Throughout the years, CT scanners have evolved into different versions or generations since their invention in 1972. They vary mainly on two factors: the construction of X-ray tubes and detectors, and the examination table's movement[18].

Spiral or Helical CT was the next milestone reached in the history of its development. This was by far one of the most significant improvements, developed by physicist W. Kalender in contribution with P. Vock et al. They addressed one issue that would not only make CT scanning faster but more accurate and comfortable for the patient. Breathing is a biological function which could not be left out of the equation, and that nevertheless had a major negative influence in the CT examinations' outcome. It led to discontinuities in the scan, which in turn failed to include several anatomical structures, prolonged the scanning time, disturbed the image quality and therefore jeopardized the diagnosis [19]. Spiral CT however,

not only shortened the time required per examination but also reduced the noise on the final image.

Helical CT provided a continuous scan that could be performed in a single breath while the table feed mechanism adapted to the continuous data acquisition[19]. Nonetheless, an important limitation was that the power of X-ray tubes had to be increased accordingly with the scan speed. Since then, CT machines have been getting better, faster, and provide better image quality as well as various options in table movement. As CT scanners progressed from single to multidetector, shorter scanning periods were enabled. This also brought new potential applications as well as significant improvements such as quantitative volume imaging and the possibility to provide functional information[20].

Nowadays, changes in CT scanners are not as tangible as its early beginnings. CT manufacturers make small changes that set them apart from their competing brands but focus mainly on comfortability for the patient, radiology technician and radiologist. The technician can modify parameters within each examination. However, each machine changes not only the denomination of these parameters but sometimes come already with predetermined protocols.

TRENDS IN RADIOLOGICAL EXPOSURE

Medical radiation exposure has become a matter of study in most nations. As imaging diagnostic tools keep evolving, and its utilization keeps growing, it has become a need to create feasible statistical data regarding its role in hospitals. An increasing tendency in medical radiation exposure was documented by the European Commission in general surveys from 2007 to 2010 in 36 European countries[21]. When compared to the USA or Australia, the radiation exposure in European countries represents about one third and one half respectively of its peers [21].

By interviewing 36 European countries and gathering their data, a total annual frequency of 660 million X-ray procedures was reported; This means 1.1 examinations per caput[21]. As expected, the distribution varies significantly from country to country. In Austria in 2015, CT examinations added up to 11% of all diagnostic imaging studies. That means 166 examinations per 1000 habitants, which is slightly higher in comparison to Germany and Switzerland with 132 and 101 examinations, respectively[22]. In the UK, a total of 4,815,200 CT scans were made between the years 2016 and 2017, showing a significant 7.9% growth in utilization since 2015[23].

The average frequency for CT examinations was found to be 8.7% per 1000 inhabitants in European countries. In contrast, plain radiography reached a mean frequency of 87.4%. Altogether, X-ray procedures in European countries have a mean collective effective dose of 1,05 mSv per caput. CT procedures represent 60% of it[21]. This high percentage highlights the importance of CT scanners in the overall diagnostic process and creates the need to regulate its use to bring radiation exposure to the minimum.

Pediatric research regarding radiation dose is a frequent topic. But to be able to quantify a collective radiation exposure, a statistical overview of X-ray procedures should be built for this age range. On its Annual Statistical Release between the years 2016 and 2017, England reported that 2,050,410 plain radiographies were made in patients within the age of 0-14 years. On the other hand, around 54,750 CT scans were made at the same age group[23]. Germany's statistical review on medical x-ray examinations provides also an age stratification. In their 2018 analysis, a total of 406,650 plain radiographies were reported. From these, 2.7% were made in patients under the age of 20 years. Regarding CT examinations, 1.18% from a total of 6,296,363 performed scans corresponds to patients 20 years or younger [24].

It requires a thorough analysis and an even greater effort to generate representative data for a group of countries, such as the European Union. Nonetheless, technology keeps evolving, radiation exposure is now a fundamental aspect of daily medical practice, and its consequences could be prevented, especially in more susceptible populations such as children.

IMAGE QUALITY

To understand how image quality is obtained in CT, three factors should be defined. The first is the spatial resolution, which determines the machine's ability to produce an image in which the radiologist can differentiate between two objects[25, 26]. "A high spatial resolution is important for one to discriminate between structures that are located within small proximity to each other" [25].

The second is the contrast resolution, which refers to the ability to distinguish between differences in image density[27]. By adjusting diverse machine parameters or by using contrast medium (CM), contrast resolution can be modified[26, 27]. These parameters are further discussed in this work.

The third is the temporal resolution which intends to avoid image blurring due to motion artefacts. A high temporal resolution can be achieved by a fast X-ray tube rotation and therefore a fast data acquisition. Focused and specialized reconstruction algorithms are used to improve its results[26]. Image quality is a quality standard, which results from rendering the CT's delivered information[28].

DIAGNOSTIC REQUIREMENTS

According to the European Guidelines on Quality and Criteria for Computed Tomography, imaging criteria can be of two types: anatomical and physical. The anatomical criteria consider "…anatomy in the examined areas and the contrast between different tissues to detect pathological changes". Physical criteria refers to all objective measurements in an examination[29].

PHYSICAL AND TECHNICAL PARAMETERS WITH IMPACT ON IMAGE QUALITY

Image quality is the result of a series of physical and technical features. These features can be adjusted within every CT machine to answer the primary clinical question. Adjustments on the following parameters, keeping in mind the ALARA (As low as reasonably achievable) principle, assures the minimum required radiation dose per study.

Noise

One of the main factors influencing image quality is image noise. As one of its most simple definitions, "Noise arises as random variations in the recorded signal (...) from pixel to pixel"[26]. Furthermore, its data is presented as a standard deviation of mean enhancement (calculated from the voxel values within the image data)[30] and is influenced by numerous parameters, such as mAs, slice thickness and patient size[25]. High image noise decreases image quality and hinders contrast resolution[25].

Slice Thickness

Slice thickness is chosen according to the clinical question and is given in millimeters. Its value is directly proportionate to low contrast resolution but inversely proportionate to high contrast resolution ("...ability to observe contours of small objects within the scanned volume"[26]). At the same dose, images with smaller slice thickness are significantly affected by image noise[29].

Pitch

Pitch is a commonly used term in helical CT, and its definition varies depending on the type of CT scanner[27, 31]:

Single Slice CT (SSCT): called detector pitch, it is defined as table distance travelled in one 360° gantry rotation divided by beam collimation[31]. With a pitch = 1.0 X-ray beams are contiguous for adjacent rotations[31]. Lower pitch values result in better image quality, but at the cost of an increase in local and integral radiation dose for the patient[29]. The opposite applies to pitch > 1.0, which lowers image quality and radiation dose[31].

Multislice CT (MSCT): called beam pitch and defined as table distance travelled in one 360° gantry rotation divided by the total thickness of all simultaneously acquired slices[27, 31].

Exposure Factors

Factors such as tube voltage (kV), tube current (mA) and exposure time (seconds) play a central role when creating scanning protocols. Nonetheless, it is important to consider that although an increase in these parameters highly improves image quality, it also increases radiation exposure[26, 29, 30].

In the newest CT machines, the strength of the beam can be altered by a feature called tube current modulation[32]. The current of the X-ray tube is modulated depending on the signal to noise ratio. This serves the purpose of maintaining a near-constant signal to noise ratio in the image across different areas of the body with varying thicknesses[32]. Excessive radiation doses are avoided while maintaining image quality[32].

ESTIMATIONS OF RADIATION DOSE

EFFECTIVE DOSE

A gray (Gy) is the unit of measurement used to represent absorbed dose. It represents the ionizing radiation (energy) per unit of mass[27, 32, 33]. However, this measurement is insufficient in terms of biological effect. For the latter, appropriate weighting factors are needed to quantify an effective dose[27, 32, 33].

“The effective dose is used to compare the stochastic risk of non-uniform exposure to radiation”[27, 34]. Carcinogenesis occurs at a different rate according to body tissue, and the effective dose represents this risk in the tissue of question[27, 34]. The following measurements are used in the attempt of measuring absorbed radiation dose per examination.

CT DOSE INDEX (CTDI)

The CTDI is a standardized measure of radiation dose output by using a cylindrical phantom, which allows the user to compare the radiation output of different CT scanners [35]. Initially, the concept was introduced by Shope et al. in 1981, using polymethyl methacrylate phantoms of 15cm length with 16 and 32 cm diameter [8, 35, 36]. CTDI was defined "(…) as the integral of the single scan radiation dose profile along the z-axis, normalized to the thickness of the imaged section ("slice thickness")"[35, 36].

It is measured in mGy, which is obtained by multiplying the CTDI normalized value by the mAs product Q used in the examination divided by the pitch factor. The previous has the benefit that it also considers the spiral CT. The resulting value provides CTDIvol[8]. "In the past CTDI100 (measured over a 100 mm long ionization chamber) and CTDIw (weighted average of dose across a single slice) were used"[32, 33, 37]. Providing CTDIvol values is obligatory in all CT scanner consoles. Nonetheless, further parameters are needed to provide optimal dose estimates. CTDIvol neglects to provide dose information according to patient size and cross-section as well as length[8].

DLP (DOSE-LENGTH PRODUCT)

DLP derives from a CTDIvol value. It multiplies the length of the study (range) with the given CTDIvol. The obtained value is expressed in mGy·cm and serves as an aid to calculate patient dose. A drawback of this value, also true for CTDIvol, is that it only provides rough dose patient estimates based on phantom measurements but does not provide an effective dose[8].

CTDIvol is then relevant to consider the patient dose burden per sequence, and DLP calculates this burden for the complete CT examination. A major advantage of both values is that they are always easily accessible from the radiation report and CT console and therefore are fundamental in the comparison of dose levels, accepted as diagnostic reference levels (DRL)[1, 8].

EFFECTIVE DIAMETER AND SSDE (SIZE-SPECIFIC DOSE ESTIMATE)

As said before, CTDIvol and DLP values fail to provide a patient size specific delivered dose. That meant that for smaller patients, the dose levels could be underestimated "(…) by a factor of 2-3 if the 32 cm PMMA phantom was used for reference"[38]. To this end, the AAPM merged the already given radiation output with patient measurements to create a Size-Specific Dose Estimate (SSDE).

The effective diameter is a crucial part in calculating the patient's SSDE and derives from the patient's diameter in a specific location along the z-axis[38]. The previous assumes the patient to be elliptical in the cross-section and calculates this diameter with the patient's lateral and anterior-posterior dimension[38]. Furthermore, the AAPM developed phantom specific tables and an equation to calculate SSDE. Although this is still an estimate, it provides the radiologist with a better tool to reduce radiation in pediatric CTs.

RADIATION DOSE RISKS

The increasing need for CT examinations made radiological protection more challenging which consequently arose the discussion of dose-dependent potential risks. This topic was already being discussed since the late '80s by Fearon and Vucich, were they analyze organ-absorbed radiation dose in children[39]. In the '90s by studies it was further addressed by research studies such as those from Mini et al. and Van der Bruggen-Bogaarts et al[6, 7]. Nowadays, data is produced at a higher speed rate, and availability of such studies is now the trend. Researchers have, therefore, over time focused more and more on special CT applications to adapt radiation dose according to the patient's physical specifications.

The effective dose in a standard CT ranges between 1-24 mSv in adults and 2-6.5 mSv in pediatric patients[5]. Despite the lower radiation doses, the exposition to ionizing radiation can be still harmful. Acute exposition effects are hardly ever seen as a consequence of a CT examination. On the other hand, molecular damage caused by low dose radiation could have long term effects after a patient was exposed to radiation [5].

THEORIES ON RADIATION EFFECTS

There are many theories and views on how ionizing radiation can damage the human body. When referring to biological effects, it can be categorized into the somatic and the hereditary effects. The following chart (Fig.1) summarizes these concepts[5, 8, 26]:

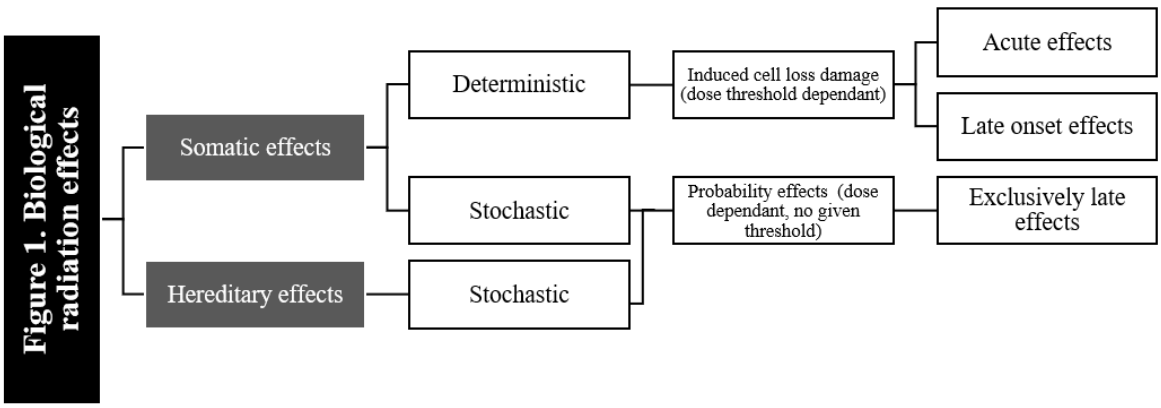

RADIATION-INDUCED CANCER

More than a century ago, the first radiation-induced cancer was reported[40, 41]. Tragedies such as the atomic bomb and nuclear plant tragedies have helped in our understanding of radiation-induced carcinogenesis[41]. However, with the advance of diagnostic imaging and interventional radiology, attention was brought to a more specific subject: effects of low-dose (<0.1Gy) ionizing radiation[42].

In an effort to create a risk to benefit ratio on this matter, epidemiological data were compared between populations exposed to low radiation doses and unexposed populations. The previous showed no significant difference in the populations' incidence of cancer development[5]. Consequently, two theories developed: one that believes there is a threshold value of radiation dose, under which no risk is shown. The other theory believes in a dose-dependent risk, the linear no-threshold theory (LNT)[5].

Studies like those of Lubin et al. support the LNT, while others like Siegel et al. strongly disagree arguing that people are annually subjected to variable but possibly higher radiation doses due to background natural radiation in comparison to those obtained through X-Rays.[10, 43–45]. In other words, these studies argument that environmental radiation is highly variable and sometimes even higher than that obtained through a radiological examination. Although there is no consistent evidence that supports or denies LNT, it is prudent to follow this model as a basis of radiation protection policy[4, 5][41]. Alongside the ALARA principle, it seems to be the more plausible solution[5, 13]. Large-scale epidemiological research studies are still being conducted, but the concerns towards a higher cancer incidence have been estimated throughout various reports supporting existing radiation-induced cancer theoretical models[3].

Spontaneous cancer development is subjected to probability. To classify a malignant disease as radiation-induced cancer, the most common types of spontaneous cancer must be analyzed[5]. Having observed an increase in said cancers associated with previous radiation exposure supports the fundamentals of the LNT[3, 5, 8]. Meaning that "each specific cancer will have its level of radiation risk dependent on its spontaneous incidence"[5]. This, in turn, may also be population specific.

Acute radiation exposure can lead to short- and long-term cancer development by a series of cell mutations over time[5]. Ionizing radiation interacts with the tissue following several mechanisms of DNA damage. Unrepaired or misrepaired DNA has proven to lead to

mutations and chromosome damage[26]. Said mutations might lead in coming years to malignant diseases, hereditary effects or cellular damage (cellular senescence, necrosis or apoptosis). The inflicted damage and the recovery depend on the tissue's radiosensitivity and the radiation dose[5, 26].

CT RADIATION EXPOSURE: THE PEDIATRIC ISSUE

Undeniable as the risks from radiation exposure are, this study intends to focus on the pediatric community. The increasing use of diagnostic imaging has led to rising concerns towards radiation exposure in children. The deleterious effects of ionizing radiation seem to have greater consequences for younger patients. The first thing to consider is the dimensions of a young patient. A child's weight varies since birth starting with just around three kilograms until puberty when it reaches an adult's weight[9]. Furthermore, according to several research studies, not only does weight dramatically vary but also mass composition, as well as distribution and maturation of tissues. Weight is, therefore, not the most accurate parameter for developing pediatric CT scanning protocols[9, 46].

Another important factor is the rate of tissue proliferation, which is at its maximum in children. Consequently, this presents a higher tissue vulnerability to radiation and increases the risk not only of radiation-induced cancer development but also the risk to develop a lethal form of cancer[5, 11]. Children's life expectancy is doubtless longer as the one expected in adults. Cell mutation derived from radiation experiences will develop through time, and therefore the probability of developing cancer years after exposure is more probable to be seen in younger patients[5, 47].

Normally, children tend to have less fatty tissue, especially visceral fat. This affects low contrast resolution, which means the need of higher radiation dose to obtain better image quality. In the last two decades, however, fat tissue has also been of relevance in children. The quantity of overweight children has substantially risen, showing an estimate of 20% of Europe's school-age children. Additionally, one in five of said children present obesity[48]. Therefore reports have also focused protocol adjustments to overweight and obese children[46].

Radiation exposure poses a high risk, particularly to children younger than one year of age. Various studies suggest that due to children's radiation vulnerability, they present with a lifetime risk of developing one cancer every 500 scans (abdominal and pelvic CT scans), regardless of age at exposure [49]. Another study conducted in Australia (one of the

countries with most CT scan performance) compared two pediatric cohorts, the first group with at least one CT examination while the other group had none. After a 9.5 years average follow-up after exposure, it was concluded that exposed children had an overall higher cancer incidence of 24% [50]. Furthermore, several studies have reported a strong link between radiation exposure in pediatric patients and the development of leukemia and brain tumors. Within these, the increased risk of developing said pathologies after low-dose radiation exposure was reassured[51, 52].

RADIATION DOSE OPTIMIZATION ATTEMPTS

A collective effort has been made not only by the radiology team but also by CT manufacturers in the development of strategies and better protocols to reduce applied radiation dose.

It is essential to remember that MRI and ultrasound represent a viable alternative for CT, pose no radiation threat and therefore, should be preferred as a first-line diagnostic tool. Children present a different pathology incidence to the adult population, which should also be considered in said protocols. The newest CT scans offer faster scanning times, better resolution, dose modulating tools and dose shaping filters, as well as several other advantages[5].

As mentioned before, modulating tube voltage and tube current influence greatly received radiation dose and therefore must be adapted to pediatric protocols[53]. As part of the new developments in CT scanning protocols and aiding tools, iterative reconstruction techniques (IRT) have slowly replaced traditionally used filtered back projection (FBP) techniques, providing better image quality and better radiation dose optimization[13]. Lastly, the use of a contrast enhancement agent has also proven handy, especially for angiographic focused examinations[12].

Pediatric dose reference levels are available as guidelines to develop scanning protocols according to the ALARA principle[1]. An acceptable radiation dose range helps to avoid unnecessary radiation exposition and to create minimum standards that certify an institution as a CT centrum[22].

When considering all the available information to date, protocols can be optimally adapted for a pediatric population. Image noise ranges, that are diagnostically relevant, would be the next step to take in the development of pediatric scanning protocols. This analysis aims to create new data in this field, which could be further helpful in the development of fore

mentioned protocols and become part of today's diverse options to optimize CT radiation exposure in children.

MATERIALS AND METHODS

STUDY SETTING

This study used data obtained at the University Hospital Graz. As a retrospective study, a database was built, which contained CT examinations performed between the dates of May 2009 to February 2019. Inclusion and exclusion criteria from the different studies were met, as well as the age range. The studies are to be found in the Picture Archiving and Communication System (PACS) available at the Pediatric Radiology Department.

SAMPLE

The sample of this study was built from pediatric patients, who in the past ten years had a clinically indicated CT examination performed. A database of more than 600 studies was built from the PACS available at the Pediatric Radiology Department. Inclusion and exclusion criteria are depicted in Fig. 2. Furthermore, all chosen CT scans were diagnostic.

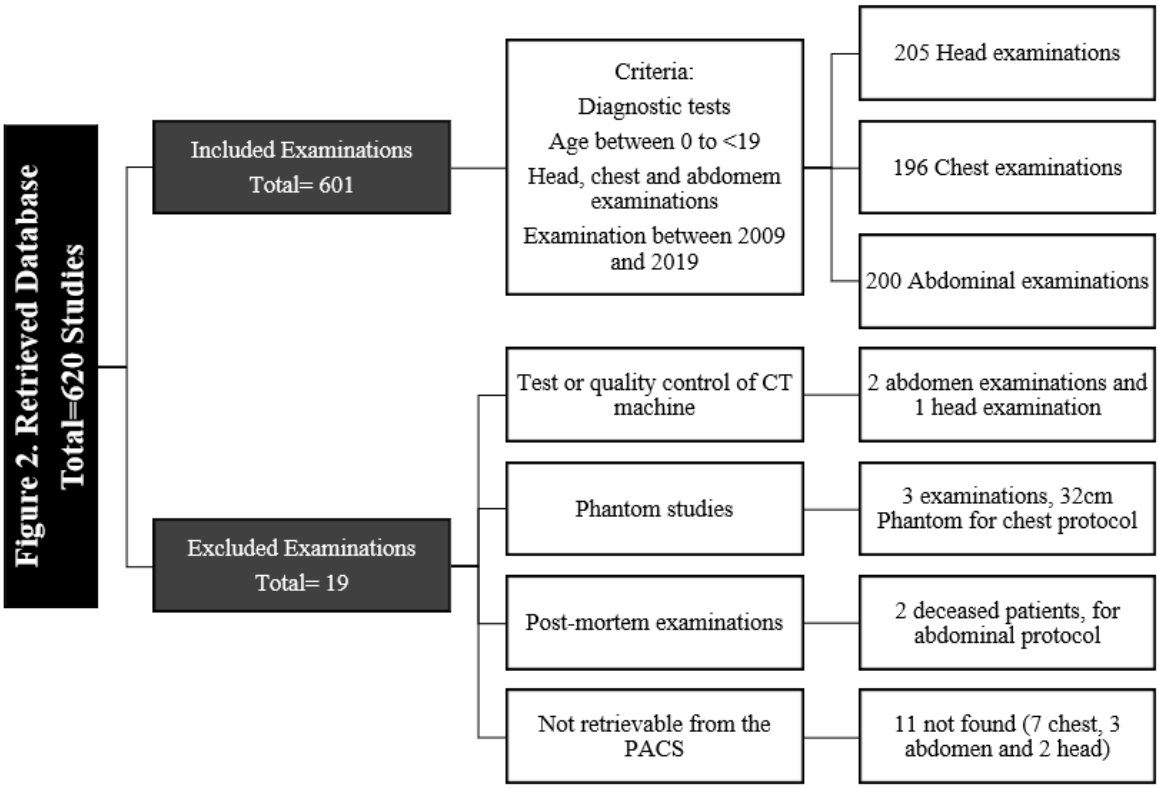

To ensure a statistical representative sample, an equal number of studies were included per examination area and per age group.

ANONYMIZATION

An important part of any research is to ensure the data protection of every participant. This study required a significant amount of examinations with personal and private data from patients. Therefore, it was of great importance to perform it while ensuring the anonymization of the obtained information. The data collection was done within the hospital pediatric radiology department. Examinations' data was documented in a Microsoft Excel table for later analysis and saved under password, making it accessible only to the lead researcher and both supervisors. It was then kept in the department's computers. Names, dates, as well as specific identification numbers, were erased for further statistical analysis. This left just the raw data to analyze and therefore, the safety to do so outside hospital premises.

MEASURES AND PROCEDURES

For each anatomical area, specific structures were defined from which a region of interest would be measured. The following chart (Fig. 3) exemplifies the ROIs per region:

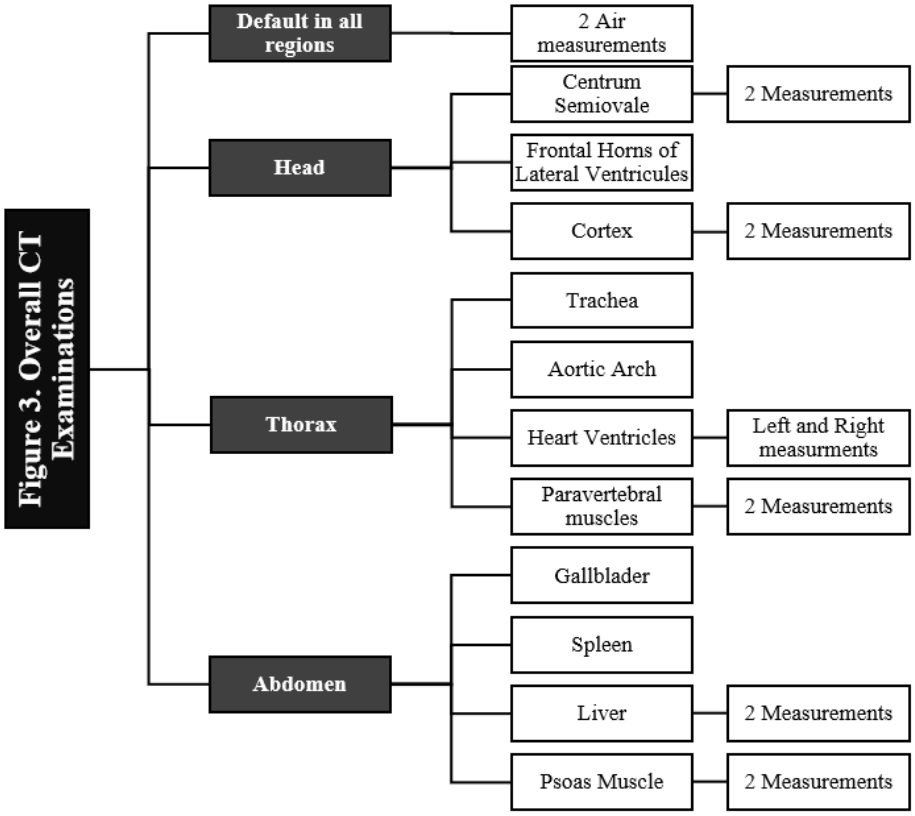

A default measurement for all regions was included. Therefore, two measurements of background noise (air) were taken accordingly.

Once defined, images were then assessed aided by the syngo.plaza PACS software available at the department's computers, where circular measurements of the different regions of interest (ROI) were made. The aim size of the measurement was 125 mm^2 based upon similar research studies[46, 54, 55]. According to de AAPM 39th report, noise is measured by the CT machine and given as the standard deviation of pixel values within a ROI on a scan of a water phantom[54]. Mean standard deviation of ROI's was documented as the image noise in this study. Figures 4 to 7 depict the ROI placement per anatomical region.

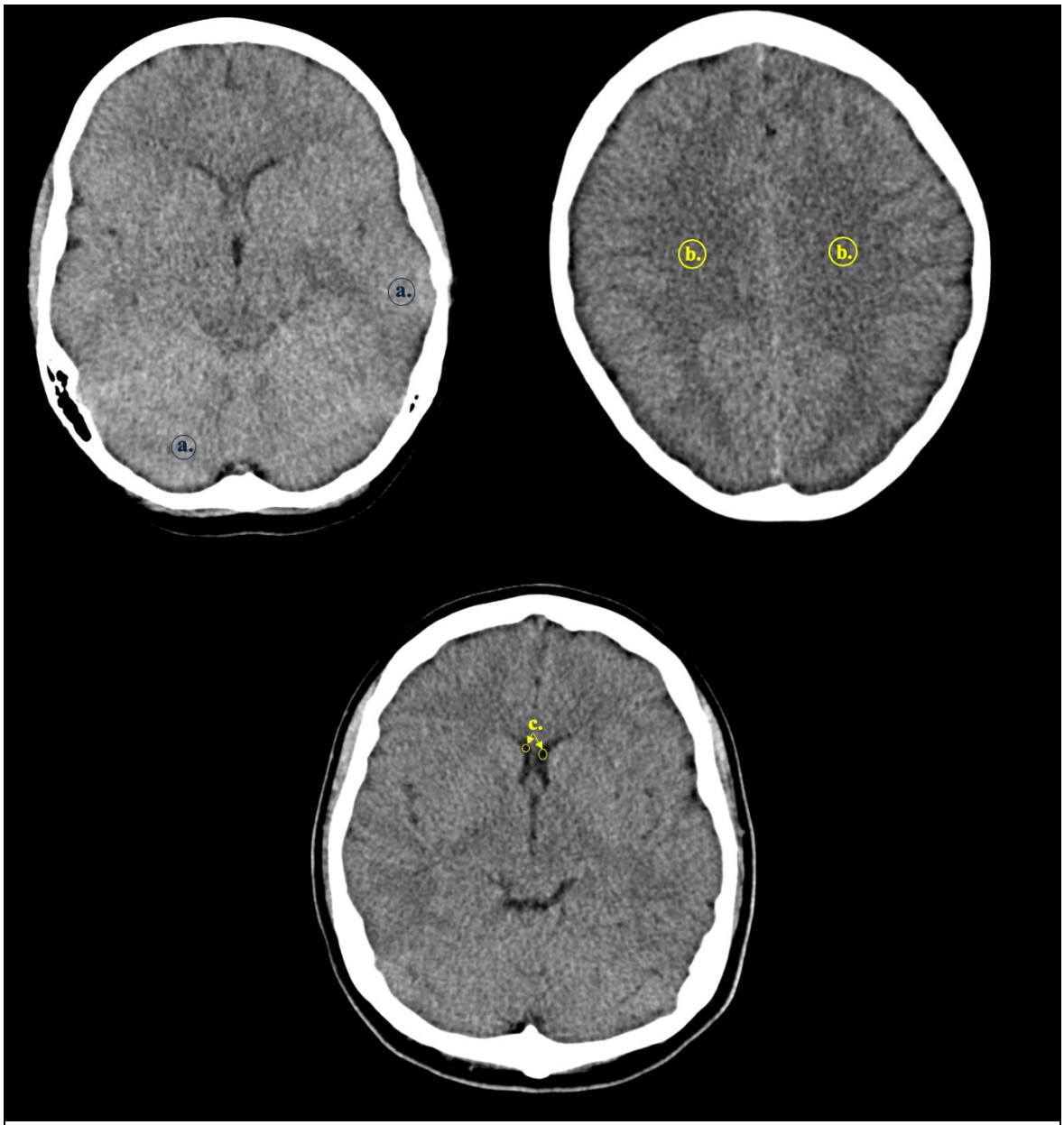

Figure 4. ROI selection in head CTs. **a.** cortex; **b.** centrum semiovale; **c.** frontal horns of the lateral ventricles

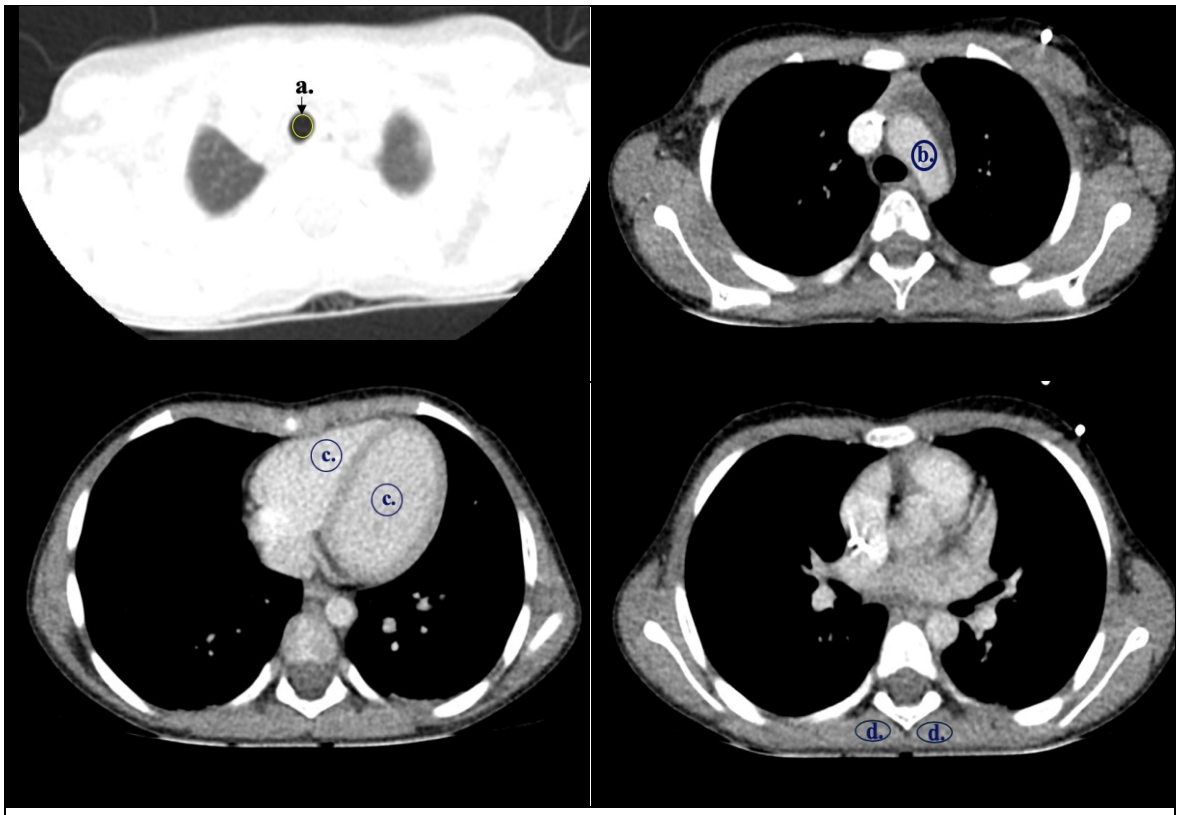

Figure 5. ROI selection in chest CT. **a.** trachea; **b.** aortic arch; **c.** heart ventricles (right and left); **d.** paravertebral muscles

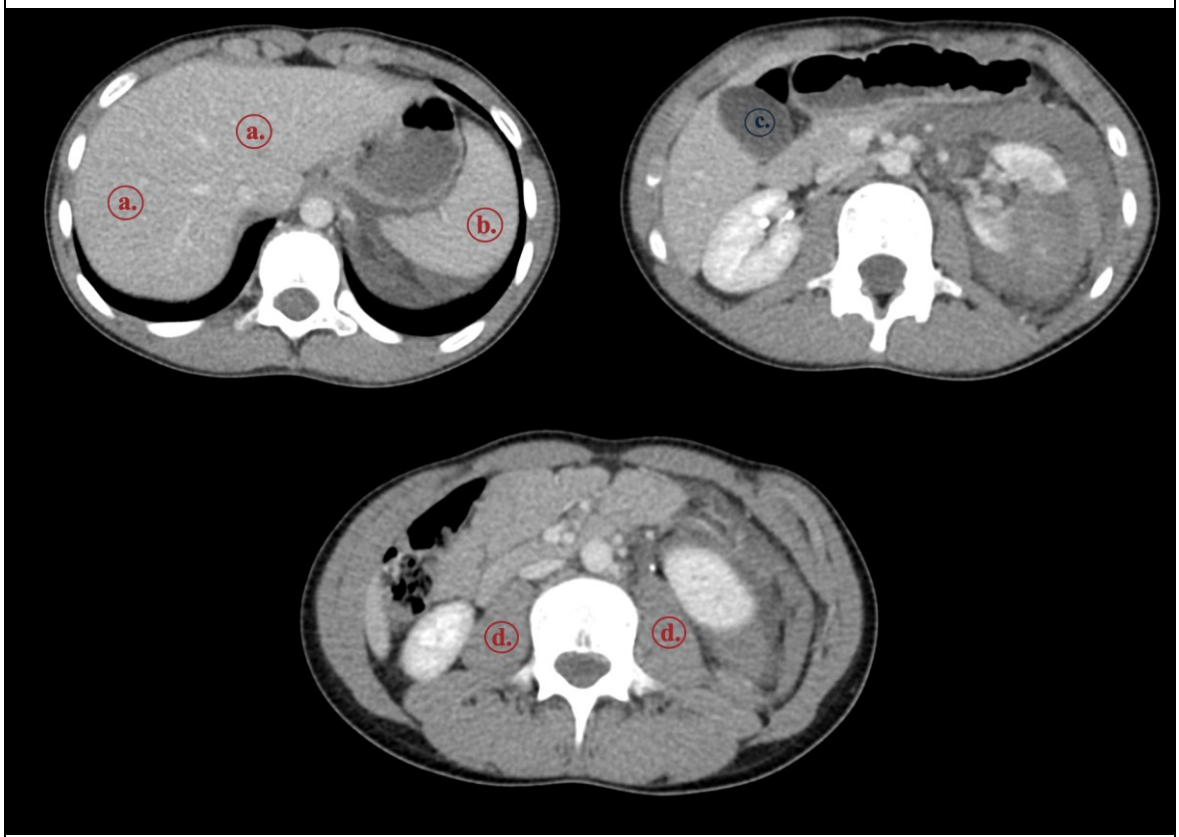

Figure 6. ROI selection in abdominal CTs. **a.** liver; **b.** spleen; **c.** gallbladder; **d.** psoas muscle

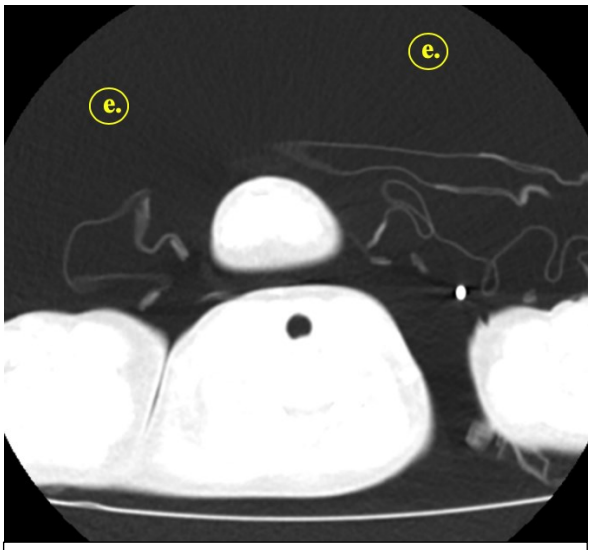

Figure 7. Background ROIs

The measurement of the noise was made by searching for a homogenous area where the ROI was located. This was an especially difficult task in subjects younger than one year. Although larger surfaces have more statistical relevance, ROI size had to be adjusted when homogenous noise was not found. Furthermore, the outlining of the specific anatomical structures was of high importance to produce feasible data. Measurements were therefore not made when the anatomical structure could not be precisely identified. These missing cases are addressed separately per region in the "Results" section of this study.

To ensure correct ROI placement, HU were measured within each of them. In the Hounsfield scale, the CT value -1,000 HU is assigned to air and the CT value 0 HU to water [18]. The applied tube voltage determines variations of the HU values and this effect can be observed, for example, in enhanced tissue or bone[26]. Table 1 served as a Hounsfield scale guideline[26].

Table 1. Typical HU values and ranges of values for different tissues and materials

Substance	HU
Compact bone	+1000 (+300 to +2500)
Liver	+60 (+50 to +70)
Blood	+55 (+50 to +60)
Kidneys	+30 (+20 to +40)
Muscle	+25 (+10 to +40)
Brain, grey matter	+35 (+30 to +40)
Brain, white matter	+25 (+20 to +30)

Water	0
Fat	–90 (–100 to –80)
Lung	–750 (–950 to –600)
Air	–1000

Additional data was recollected from each specific evaluated examination series such as kV, slice thickness, CTDI and DLP. Furthermore, AP and lateral distances were measured from each series on the axial projection, and effective diameter was calculated according to the following equation[38]:

$$effective\ diameter = \sqrt{AP\ x\ LAT}$$

Afterwards, with the obtained effective diameter, value conversion factors were obtained by consulting the tables provided in the Report 204 by the American Association of Physicists in Medicine. A corresponding SSDE to each examination was also calculated with the aid of the equations provided in the AAPM 204 RPT[38]:

$$SSDE = f^{\frac{16X}{size}}\ x\ CTDI^{\frac{16}{vol}}$$

$$SSDE = f^{\frac{32X}{size}}\ x\ CTDI^{\frac{32}{vol}}$$

The first equation is adjusted for 16cm phantoms, and the second is for 32cm phantoms. The f refers to the conversion factor according to each specific phantom size.

SUBJECTIVE EVALUATION

An important part of this study was a thorough subjective evaluation of the image quality. Aided by experienced radiologists and based on the European Guidelines on Quality Criteria for Computed Tomography, two evaluation scales were created, and all 601 examinations were classified within the given criteria. Given the nature of this work, the examinations were only judged by the lead researcher, whereas in similar studies at least two experienced pediatric radiologists perused the CT scans as well[46]. CT scans were graded subjectively according to the following scales:

Table 2. Subjective analysis of overall image quality		
Optimal	Acceptable	Unacceptable

Figures 8 to 10 exemplify the subjective analysis of overall image quality:

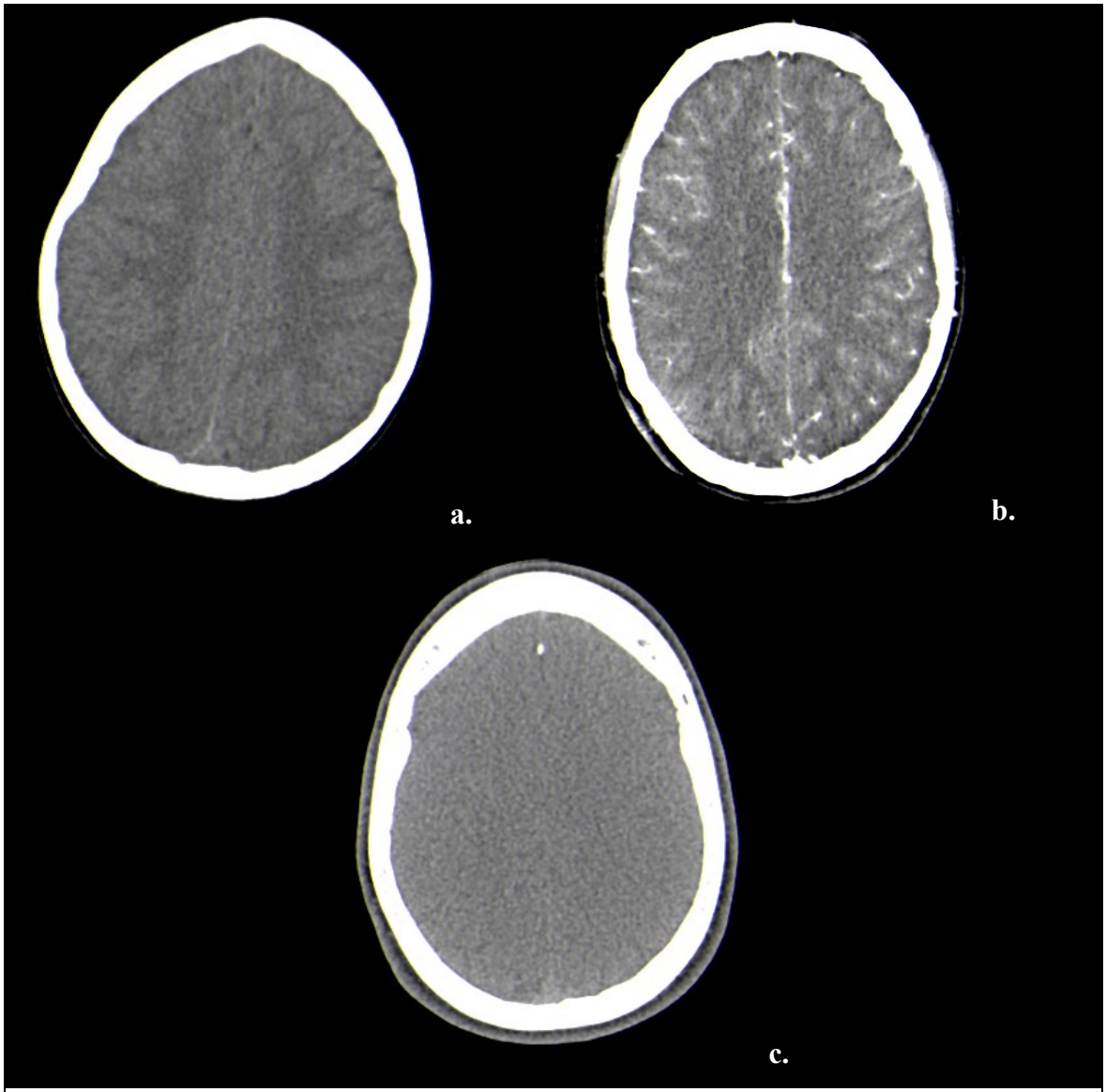

Figure 8. Examples of subjective analysis of overall image quality in head CTs. **a.** optimal **b.** acceptable **c.** unacceptable

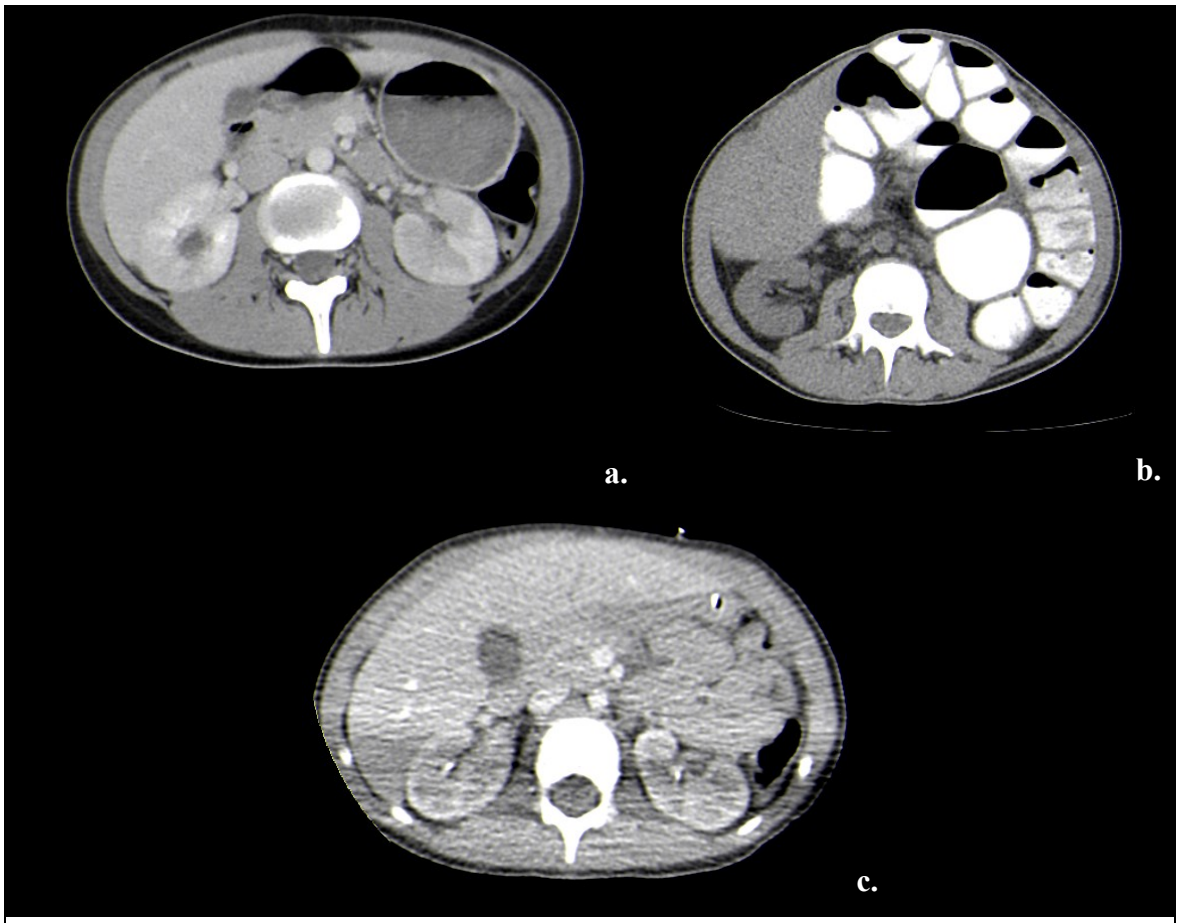

Figure 9. Examples of subjective analysis of overall image quality in abdomen CTs.
a. optimal **b.** acceptable **c.** unacceptable

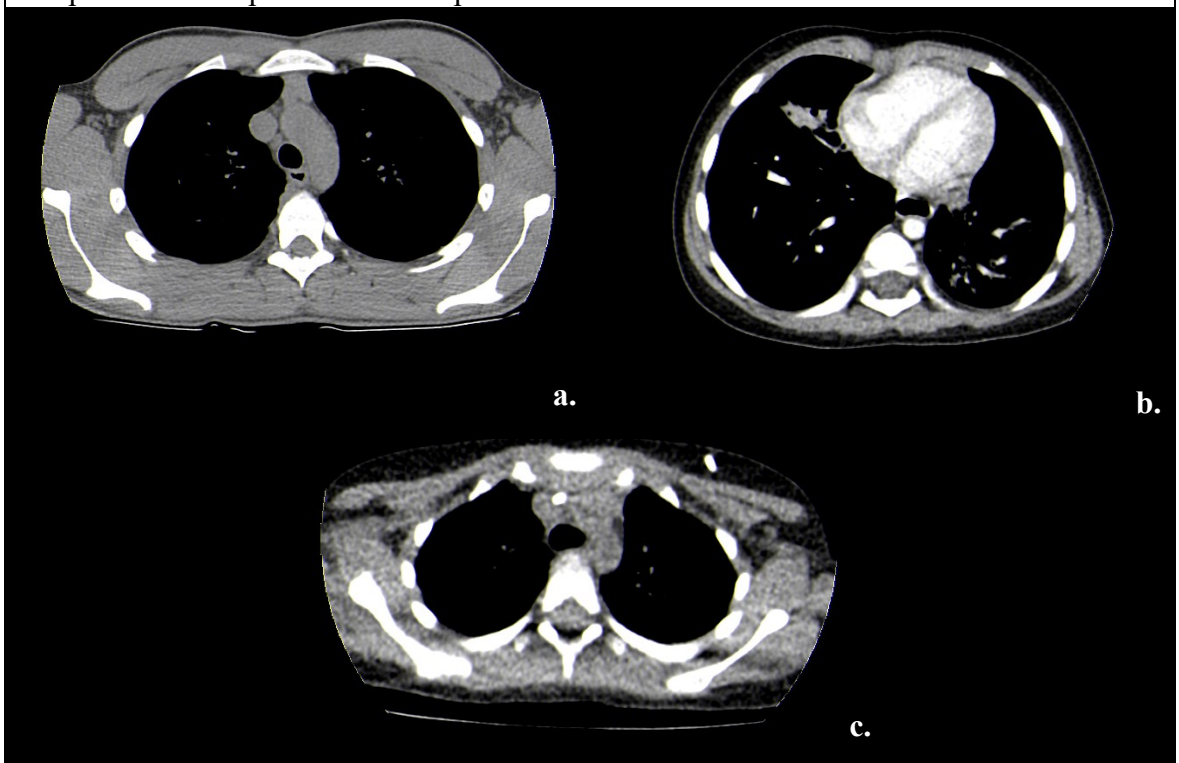

Figure 10. Examples of subjective analysis of overall image quality in chest CTs.
a. optimal **b.** acceptable **c.** unacceptable

Table 3. Subjective noise analysis					
None	Minimal	Low	Moderate	Significant Noise	Excessive Noise

Figures 11 to 13 provide examples for the subjective noise analysis.

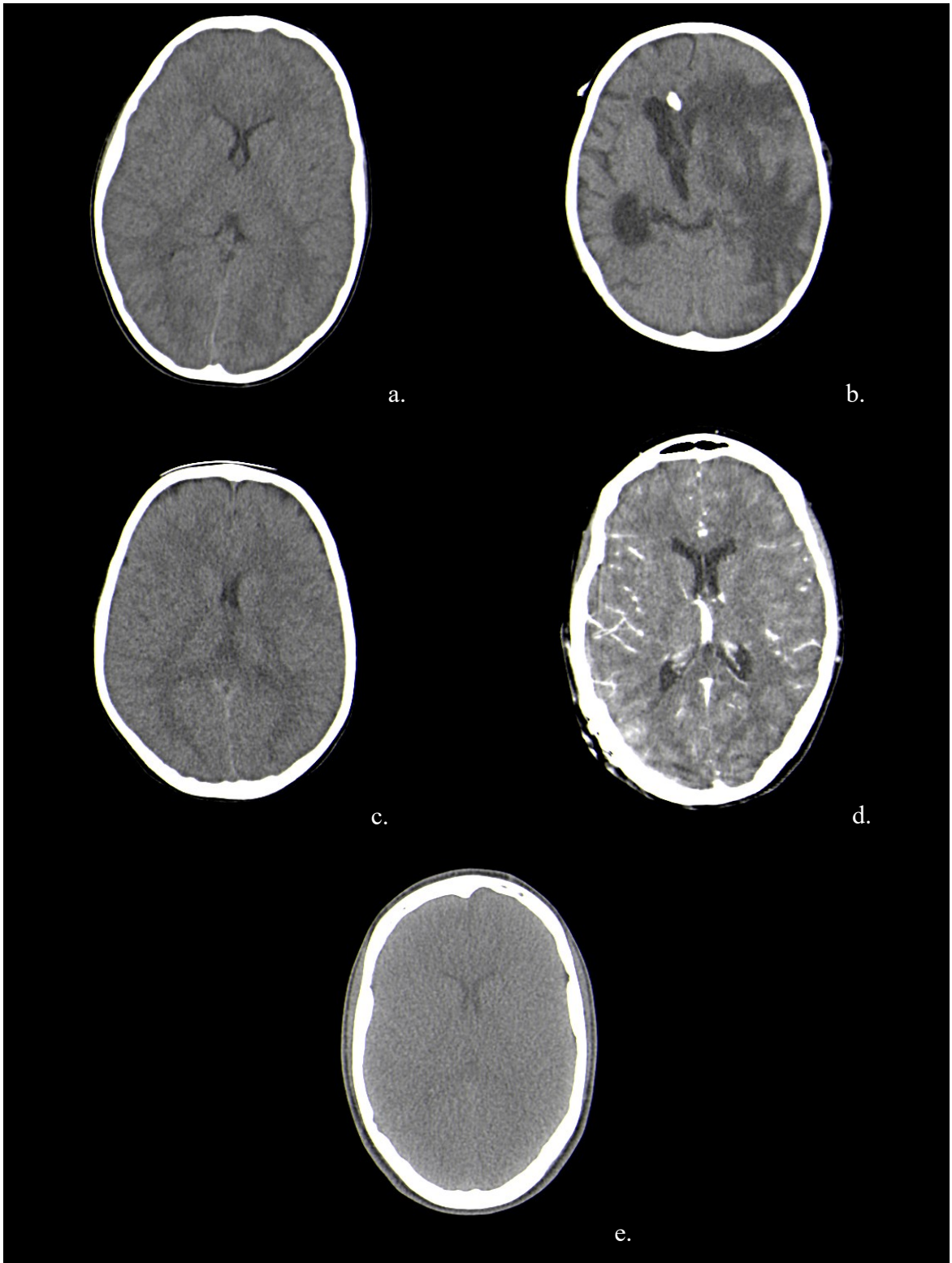

Figure 11. Example of subjective noise analysis in head CTs. **a.** minimal **b.** low **c.** moderate **d.** significant noise **e.** excessive noise

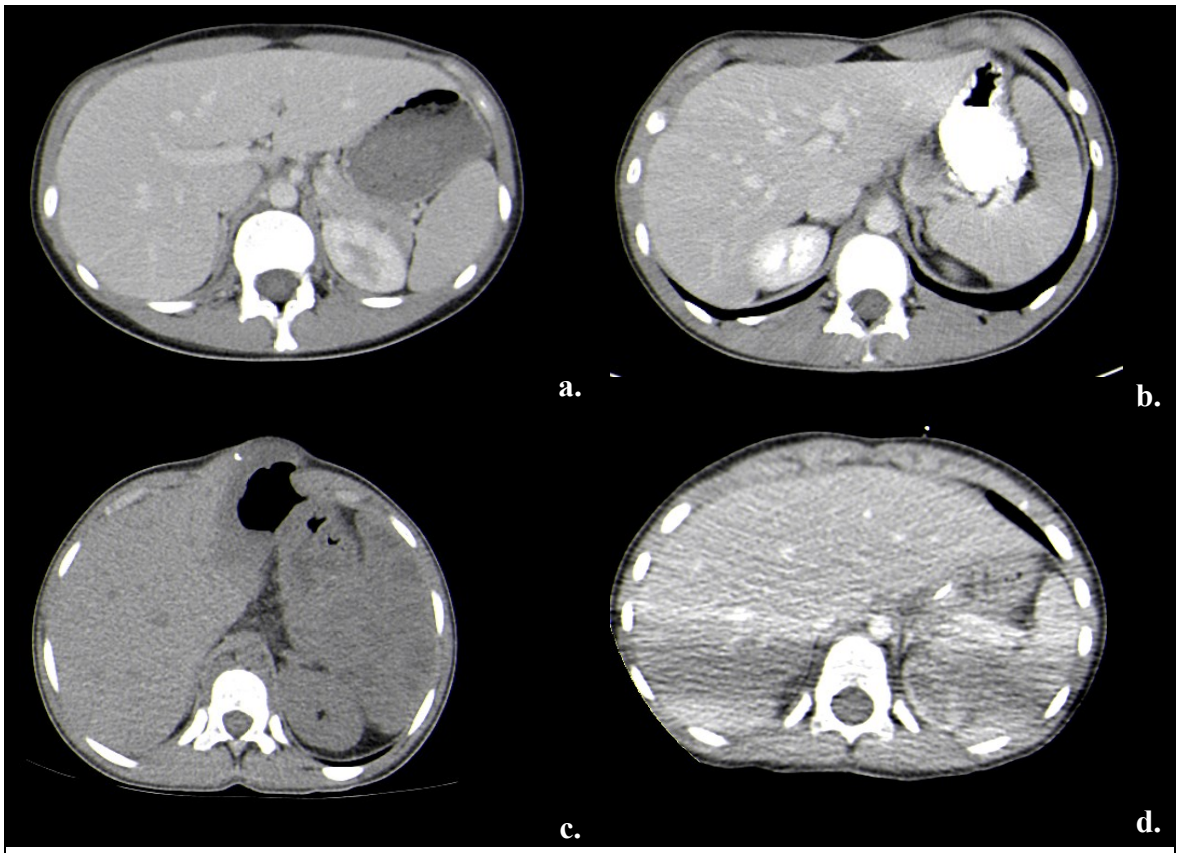

Figure 12. Example of subjective noise analysis in abdomen CTs. **a.**minimal; **b.**low; **c.**moderate; **d.**excessive noise

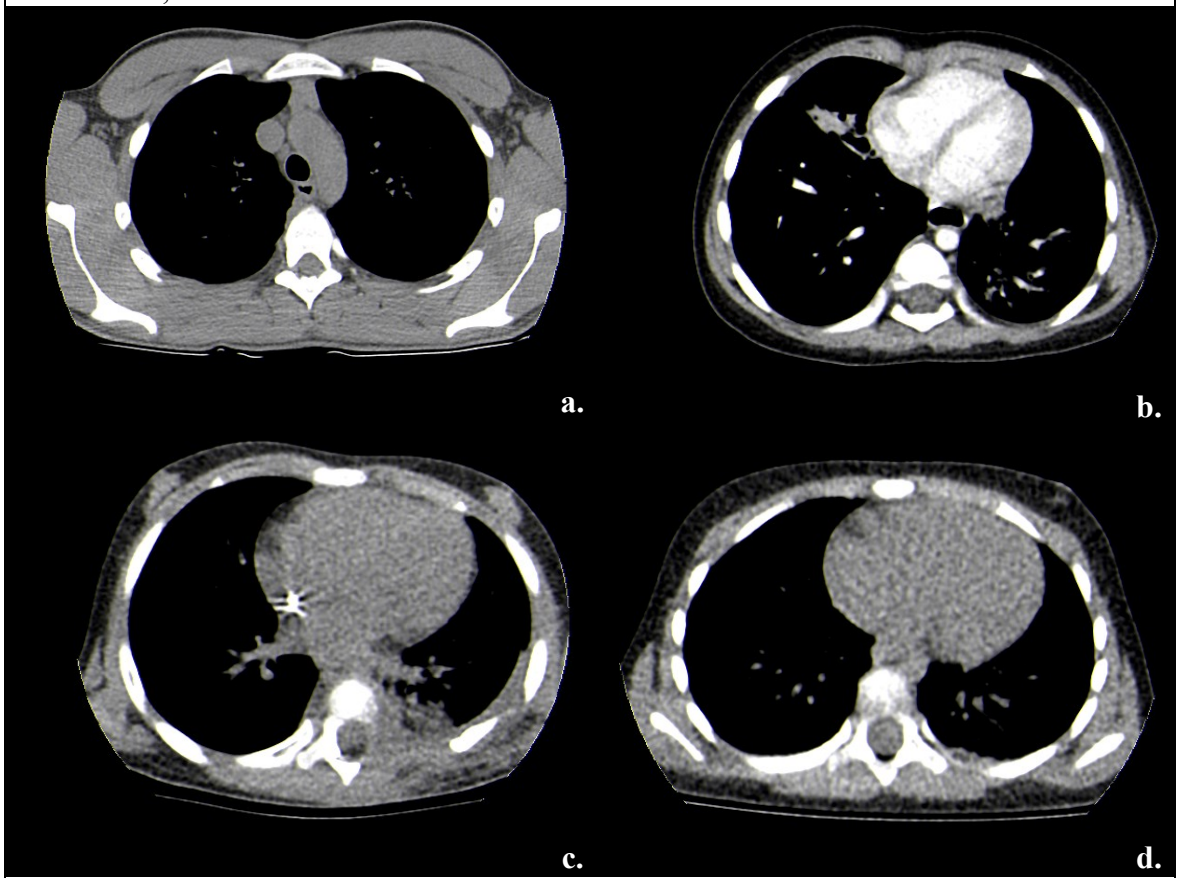

Figure 13. Example ofsubjective noise analysis in chest CTs. **a.**low; **b.**moderate; **c.**significant noise; **d.**excessive noise

To ensure a homogenous analysis, all CT images were reviewed in axial slices as well as in the same series where the objective measurements were made. Although as part of the inclusion criteria examinations had to be diagnostic, the lead researcher evaluated according to her knowledge the diagnostic acceptability.

STATISTICAL ANALYSIS

OBJECTIVE DATA ANALYSIS

The data were analyzed with IBM SPSS Statistics version 25.0 virtual software provided by Medical University Graz. For all performed tests, the level of significance was defined as $p < 0.05$. Descriptive statistics were used to analyze datasets.

The Kolmogorov-Smirnov test was run to assess the data's distribution. According to the resulting distribution, parametric tests (Independent Samples T-test), and non-parametric tests (Mann Whitney U-test) were used. For the descriptive statistical analysis, numeric values were reported as mean ± SD, for a normal distribution, and median (95% CI of the mean), for not normal distributions.

The data was arranged in subgroups to perform the analysis. Data was first divided per region, and within each region, subgroups were formed according to the measured parameters.

SUBJECTIVE DATA ANALYSIS

Subjective data was also tested with the Kolmogorov-Smirnov test. A descriptive statistics analysis was also performed. To report obtained numeric values, mean ± SD was used for normal distributions and median (95% CI of the mean) for not normal distributions.

RESULTS

BASELINE DATA

Diverse data was retrieved from the examinations. Patients within this study ranged from newborn age to less than 19 years old. The youngest patient was a newborn, and the oldest was 18 years and 11 months. For practical and study reasons, they were divided into five groups according to age. Age groups were built based on PiDRL Guidelines[1] and adjusted, as seen in Table 4.

Table 4. Age Groups Division and Mean Age

	GROUP 1	GROUP 2	GROUP 3	GROUP 4	GROUP 5
Age Range	0 to <2	≥2 to <5	≥5 to <10	≥10 to <15	≥15 to <19
Median (95% CI)	0,8 (0,8-1,1)	3,5 (3,4-3,7)	7,6 (7,4-7,8)	12,9 (12,5-13,0)	17,6 (17,2-17,6)
Male	34 (54%)	51 (57%)	70 (47%)	95 (62%)	80 (54%)

CI: Confidence interval

Figure 14. Number of Patients per Age Group

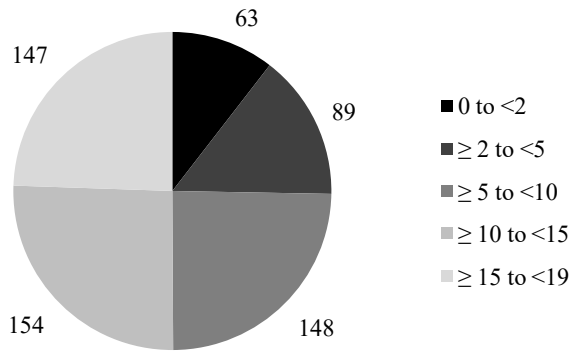

For all groups, except age group 3 (≥5 to <10), patients were predominantly male. In total, from overall examinations, male patients represent up to 55% (n= 331) of the analyzed data and female patients came up to 45% (n= 270) of the data.

Figure 14 depicts the number of examinations within each age group. The major number of examinations were found in group 4 (≥10 to <15), with 154 examinations. In contrast, only 63 examinations were retrieved in the age group from 0 to <2 years old.

The number of examinations per region within each age group is evenly distributed, as seen in Fig. 15. Head examinations have a higher frequency within each age group (except for group "≥2 to <5").

The diagnosis was not considered when analyzing CT scans. Therefore, patients were included more than once when they had more than one CT scan performed during the selected period (Figure 16). The lowest number of patients belongs to the age group number one, which reflects the exceptional use of CT in younger patients.

Figure 15. Number of Examinations per Age Group and Region

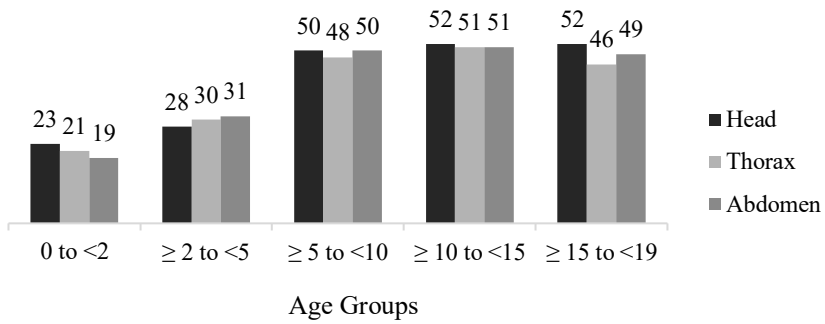

Figure 16. Examinations in chosen Time Span

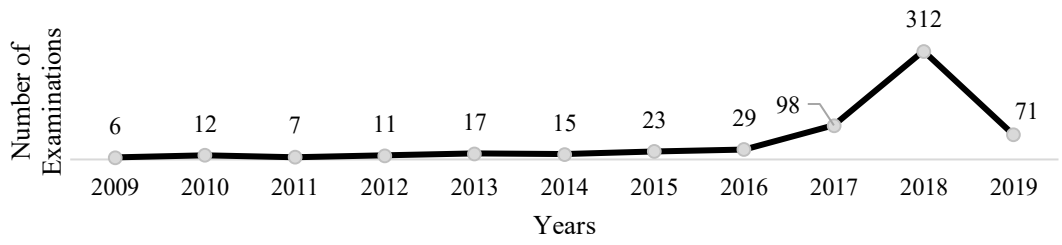

Figure 17. Native Examinations per Region

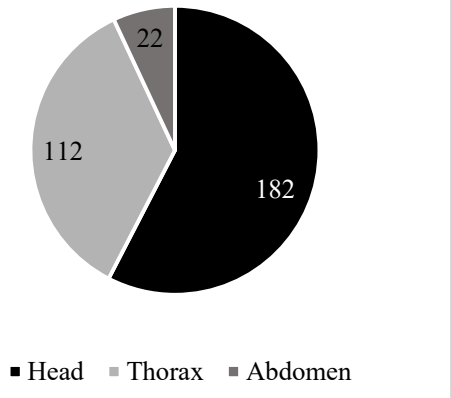

Figure 18. Examinations with the use of CM per Region

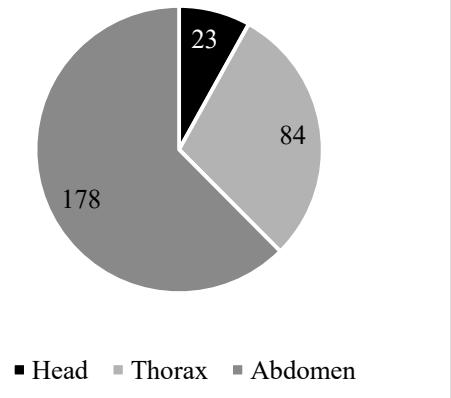

Another factor relevant to the image noise is the use of a contrast agent (Fig. 17 and 18). Head examinations were mostly done native, presenting 182 (89%) native examinations and only 23 (11%) examinations with CM. Examinations from the abdomen showed the opposite

with only 22 (11%) native examinations and 178 (89%) examinations with CM. A total of 112 (57%) were native chest examinations and 84 (43%) with CM.

Tube voltage values within the database were mainly 80 kV, 100 kV and 120 kV. Nonetheless, four abdominal examinations used a 90 kV tube voltage and just one a 140 kV tube voltage. When analyzing per region, 106 (52%) head examinations were done with a 120 kV tube voltage (Table 11). From these, 49% (52) were examinations in age group 4 (≥10 to <15) and 48% (n=51) in age group 5 (≥15 to <19). As much as 94 (46%) of the examinations were made with 100 kV, and 47 (50%) of them belonged to patients ≥5 to <10. Only 5 (2%) of the head examinations were done with 80 kV, all of them in patients in age group number 1 (0 to <2) (Table 5).

Table 5. Number of Head Examinations per Age Group According to Tube Voltage

Age Groups	80 kV	100 kV	120 kV
0 to <2	5 (100%)	18 (19%)	-
≥2 to <5	-	28 (30%)	-
≥5 to <10	-	47 (50%)	3 (3%)
≥10 to <15	-	-	52 (49%)
≥15 to <19	-	1 (1%)	51 (48%)

Regarding chest CT scans, half of the examinations (n=98) were done with a 120 kV tube voltage (Table 11). Mainly, they belonged to age groups 4 and 5 (≥10 to <15; ≥15 to <19) as seen in Table 6. A total of 84 (43%) examinations were done with 100 kV, and 46 (55%) of them belonged to patients in the age range from ≥5 to <10. Fourteen (7%) chest examinations were done with 80 kV, all of them belonging to age group 1 (0 to <2) (Table 6).

Table 6. Number of Chest Examinations per Age Group according to Tube Voltage

Age Groups	80 kV	100 kV	120 kV
0 to <2	14 (100%)	7 (8%)	-
≥2 to <5	-	29 (35)	1 (1%)
≥5 to <10	-	46 (55%)	2 (2%)
≥10 to <15	-	2 (2%)	49 (50%)
≥15 to <19	-	-	46 (47%)

Lastly, 92 (46%) examinations were performed equally at a 120 kV and 100 kV in the abdominal region. However, 47 examinations (51%) done with a 120 kV belonged to age group 4 (≥10 to <15), while most examinations (n= 42;46%) done with 100 kV, belonged to age group 3 (≥5 to <10). More detailed information is summarized in Tables 7 and 11.

Table 7. Number of Abdominal Examinations per Age Group according to Tube Voltage

Age Groups	80 kV	90 kV	100 kV	120 kV	140 kV
0 to <2	9 (82%)	-	8 (9%)	2 (2%)	-
≥2 to <5	2 (8%)	-	28 (30%)	1 (1%)	-
≥5 to <10	-	-	42 (46%)	8 (9%)	-
≥10 to <15	-	-	4 (4%)	47 (51%)	-
≥15 to <19	-	4 (100%)	10 (11%)	34 (37%)	1 (100%)

The reconstruction kernel was also documented. Thirteen different types of kernel were used in the study period. However, FC 17, 18 and 21 were mostly used. In head examinations, 187 (91%) of the studies used an FC 21 kernel. FC 18 was used in 92% (n=180) of the chest examinations and 64% (n=128) of the abdominal examinations. As much as 54 (27%) abdominal examinations presented an FC 17 reconstruction kernel. Further details are summarized in Table 11.

Slice thickness of 3,0 mm and 5,0 were frequently applied in most of the examinations. 180 head and 166 abdominal examinations were studied at a 5,0 mm slice thickness, while 182 chest examinations were studied at a 3,0 mm slice thickness (Table 11). Software version was also retrieved, being the V6.06gr006 the most frequent in all regions (Table 11). Regarding phantom size for CTDI calculations, all head and chest examinations were done with 16 cm and 32 cm phantoms respectively, whereas 29% (n=58) of abdominal examinations were done with a 16 cm phantom and 71% (n=142) with a 32 cm phantom (Table 11).

Helical CT's were standard in more than half of the examinations in all regions. Fifty-two percent (n=106) of head examinations, 86% (n=168) of chest and 89% (n=178) of abdominal examinations were spiral CT's. The median scan length in head examinations was of 160 cm, in chest examinations 228 cm and in abdominal studies 346,3 cm. Furthermore, a mean effective diameter of 15,5±1,3 cm was seen in head examinations and median values of 19,4

cm (19,2-20,5) and 20,0 cm (19,8-21,0) for chest and abdominal examinations respectively (Table 11).

Ninety percent (n=185) of the examinations in the head region had an active AIDR, in which a CTDIvol median value of 22,1 mGy (21,6-23,3) was registered. A CTDIvol median value of 38,7 mGy (36,1-39,5) was seen in non-active AIDR head examinations. In studies with active AIDR, median DLP value was of 365,1 mGy.cm (437,8-506,2) (compared to 652,8 mGy.cm [591,3-877,5] in non-active AIDR studies) and median SSDE value was of 22,4 mGy (22,2- 23,8) (non-active AIDR studies presented a median SSDE value of 37,5 mGy [35,1-38,5]) (Table 11).

Highest CTDIvol and DLP values, as well as SSDE values, are seen in older age groups (Table 8). Head examinations with active AIDR in age group 5 (≥15 to <19) present a median CTDIvol value of 28,9 mGy (23,8-25,6), while age group 1(0 to <2) had 16,8 mGy (14,3-17,1). For DLP (also in studies with AIDR), patients in the range from ≥15 to <19 years old had a 735,3 mGy.cm (549,9-725,4), while lowest DLP was seen in group 1 (0 to <2) with 234,2±59,4 mGy.cm. Highest SSDE median value was 28,4 mGy (24,7-27,3) in group 4 (≥10 to <15).

AIDR was active in most examinations, except in group 5 (≥15 to <19), where 20 examinations (38%) were done without AIDR. These examinations showed the highest radiation dose estimate values.

Table 8. Dose Estimates in Head Examinations according to Age Groups

		Group 1	Group 2	Group 3	Group 4	Group 5
		0 to <2	≥2 to <5	≥5 to <10	≥10 to <15	≥15 to <19
Total		23	28	50	52	52
AIDR active		23	28	50	52	32
Scan Length (cm, median, 95% CI)		140,0 (137,9-155,1)	160,0 (149,0-170,1)	160,0 (168,3-191,1)	215,0 (190,2-217,7)	188,8 (186,0-226,1)
Effective Diameter (mean±SD)		13,4 ±1,3	14,6 ±0,6	15,2 ±0,6	15,9 ±0,5	16,9 ±0,8
CTDI	AIDR active (mGy, median, 95% CI)	16,8 (14,3-17,1)	19,8 (18,5-21,0)	22,1 (20,0-22,5)	28,9 (24,6-27,1)	28,9 (23,8-25,6)
	No AIDR (mGy,	-	-	-	-	38,7 (36,1-39,4)

	median, 95% CI)					
DLP	AIDR active (mGy.cm, median, 95% CI)	234,2±59,4	277,8 (287,6-387,8)	380 (371,4-473,1)	693,2 (531,4-659,3)	735,3 (549,9-725,4)
	No AIDR (mGy.cm, median, 95% CI)	-	-	-	-	652,8 (591,3-877,5)
SSDE	AIDR active (mGy, median, 95% CI)	18,8 (15,9-18,9)	21,0 (19,6-22,3)	22,4 (20,7-23,2)	28,4 (24,7-27,3)	27,6 (23,1-27,9)
	No AIDR (mGy, median, 95% CI)	-	-	-	-	37,5 (35,1-38,5)

In the chest area, most of the studies were performed with active AIDR (n=193; 99%). Active AIDR chest studies showed a median value of 27,3 mGy.cm (40,1- 54,2) and 2,0 mGy (2,3-2,7) for DLP and SSDE respectively. Just three cases were performed without AIDR with a DLP median value of 241,9 mGy.cm (4,6-452,5) and SSDE median value of 13,5 mGy (-3,2-29,6) (Table 11).

Analyzed per age group, median values of each dose estimate tend to be higher at higher age ranges (Table 9). Most examinations were performed with AIDR, except for three examinations from group 5 (≥15 to <19). Examinations with active AIDR had lowest CTDIvol median value in group 1 (0 to <2) with 0,7 mGy (0,7-1,0), while group 5 (≥15 to <19) showed 2,0 mGy (2,2-3,2). Similarly, DLP and SSDE median values with active AIDR in group 1 (0 to <2) were 10,2 mGy.cm (9,1-15,3) and 1,7 mGy (1,6-2,2) respectively, while group 5 (≥15 to <19) showed 76,5 mGy.cm (78,0-117,7) and 3,3 mGy (3,3-4,5) mGy respectively. Highest dose estimate values belong to examinations performed with no AIDR.

Table 9. Dose Estimates in Chest Examinations according to Age Groups

	Group 1	Group 2	Group 3	Group 4	Group 5
	0 to <2	≥2 to <5	≥5 to <10	≥10 to <15	≥15 to <19
Total	43	21	30	48	54
AIDR active	43	21	30	48	51 (94%)
Scan Length (cm, median, 95% CI)	138,4 ±26,4	168,0 (156,9-187,5)	216,0 (209,1-226,3)	276,0 (252,3-289,6)	306,0 (288,1-327,2)

Effective Diameter (mean±SD)		12,5 ±1,4	16,5 ± 1,4	18,2 ± 1,8	22,3 ± 3,1	24,5 ± 2,8
CTDIvol	**AIDR active (mGy, median, 95% CI)**	0,7 (0,7-1,0)	0,8 ±0,3	0,7 (0,7-0,9)	1,5 (1,5-2,2)	2,0 (2,2-3,2)
	No AIDR (mGy, median, 95% CI)	-	-	-	-	9,8 (-2,2-21,4)
DLP	**AIDR active (mGy.cm, median, 95% CI)**	10,2 (9,1-15,3)	16,8 (14,9-20,9)	18,0 (19,3-24,9)	46,4 (47,6-71,6)	76,5 (78,0-117,7)
	No AIDR (mGy.cm, median, 95% CI)	-	-	-	-	241,9 (41,6-452,5)
SSDE	**AIDR active (mGy, median, 95% CI)**	1,7 (1,6-2,2)	1,7 ±0,6	1,4 (1,4-1,7)	2,4 (2,4-3,2)	3,3 (3,3-4,5)
	No AIDR (mGy, median, 95% CI)	-	-	-	-	13,5 (-3,2-29,6)

In 66% (n=131) of the abdominal examinations AIDR was active, with CTDIvol median value of 2,7 mGy (3,3-4,7), DLP median value of 93,1 mGy.cm (133,2-203,8) and SSDE median value of 3,4 mGy (4,0-5,2). In examinations without AIDR, CTDIvol median value was 4,8 mGy (4,8-7,1), DLP median value of 176,2 mGy.cm (174,8-280,7) and SSDE mean value of 8,7±6,0 mGy (Table 11)

When analyzing per age group, most examinations were done with AIDR, except in group 5 (≥15 to <19), where just 14 examinations (29%) were done with AIDR (Table 10). Higher dose estimate values were seen in older age groups. Examinations with AIDR showed a mean value of 1,8 ± 1,0 mGy for CTDIvol, a median value of 37,3 mGy.cm (23,0-61,4) for DLP and median value of 2,0 mGy (1,8-2,9) for SSDE for age group 1 (0 to <2). In contrast, these values were of 4,7 ± 3,2 mGy for CTDIvol, 190,0 mGy.cm (131,6-324,8) for DLP and 6,2 mGy (4,6-9,7) for SSDE in age group 5 (≥15 to <19).

Higher dose estimate values were seen in those examinations with no AIDR. Nonetheless, some exceptions can be seen, especially in group 3 (≥5 to <10). The previous is summarized in Table 10.

Table 10. Dose Estimates in Abdominal Examinations according to Age Groups

	Group 1	Group 2	Group 3	Group 4	Group 5
	0 to <2	≥2 to <5	≥5 to <10	≥10 to <15	≥15 to <19
Total	19	31	50	51	49
AIDR active	13 (68%)	24 (77%)	33 (66%)	47 (92%)	14 (29%)

Scan Length (cm, median, 95% CI)		210,0 ± 74,5	276,2 ± 46,2	330,0 (304,1-336,1)	400,0 (369,9-415,8)	428,0 (398,1-433,9)
Effective Diameter (mean±SD)		14,4 (12,8-17,2)	16,4 ± 1,3	18,4 (17,9-19,3)	22,9 ± 3,3	24,1 (23,5-25,1)
CTDIvol	**AIDR active (mGy, median, 95% CI)**	1,8 ± 1,0	1,6 (1,5-2,6)	2,4 (2,0-5,1)	4,2 (4,3-7,1)	4,7 ± 3,2
	No AIDR (mGy, median, 95% CI)	7,6 ± 9,7	2,3 (1,7-3,4)	2,2 ± 1,3	8,5 (0,4-13,7)	7,7 (6,6-9,3)
DLP	**AIDR active (mGy.cm, median, 95% CI)**	37,3 (23,0-61,4)	48,9 (45,2-85,5)	107,0 (74,6-202,6)	181,4 (183,9-334,7)	190,0 (131,6-324,8)
	No AIDR (mGy.cm, median, 95% CI)	54,7 (-288,9-880,9)	52,5 (30,9-100,4)	59,1 ± 31,5	327 (-5,1-581,6)	323,5 ± 131,9
SSDE	**AIDR active (mGy, median, 95% CI)**	2,0 (1,8-2,9)	2,3 (2,0-2,9)	2,9 (2,6-4,5)	5,5 (5,2-7,4)	6,2 (4,6-9,7)
	No AIDR (mGy, median, 95% CI)	4,2 (-1,4-19,5)	4,6 (3,1-6,3)	3,8 ± 1,8	12,2 (1,3-18,4)	11,6 (9,9-13,5)

Information was retrieved from the DICOM, in which just two cases in the head studies were missing, regarding DLP measurements. All previous data is summarized in Table 11.

Table 11. Retrieved Technical Data per Region

Total= 601		**HEAD**	**CHEST**	**ABDOMEN**
		205	**196**	**200**
Age Groups	**0 to <2**	23 (11%)	21 (11%)	19 (10%)
	≥2 to <5	28 (14%)	30 (15%)	31 (16%)
	≥5 to <10	50 (24%)	48 (25%)	50 (25%)
	≥10 to <15	52 (25%)	51 (26%)	51 (26%)
	≥15 to <19	52 (25%)	46 (24%)	49 (25%)
kV	**80**	5 (2%)	14 (7%)	11 (6%)
	90	0	0	4 (2%)
	100	94 (46%)	84 (43%)	92 (46%)
	120	106 (52%)	98 (50%)	92 (46%)
	140	0	0	1 (<1%)
Kernel	**FC17**	0	2 (1%)	54 (27%)
	FC18	5 (2%)	180 (92%)	128 (64%)
	FC21	187 (91%)	0	0
	Br40d\2	0	0	7 (4%)
	I30f\2	0	0	9 (5%)
	H45s	5 (2%)	0	0

	FC51	0	13 (7%)	0
	FC43	4 (2%)	0	0
	Hr44s\2	3 (2%)	0	0
	H30f	1 (1%)	0	0
	FC02	0	0	1 (<1%)
	I31f\3	0	0	1 (<1%)
	Br44d\3	0	1 (<1%)	0
Slice Thickness	**1,5**	0	4 (2%)	0
	2	1 (<1%)	7 (4%)	6 (3%)
	2,5	0	0	1 (<1%)
	3	24 (12%)	182 (93%)	27 (14%)
	5	180 (88%)	3 (2%)	166 (83%)
Software	**V6.06gr006**	185 (90%)	193 (99%)	83 (42%)
	V3.35GR006	11 (5%)	2 (1%)	19 (10%)
	V4.74ER004	0	0	55 (28%)
	Other	9 (5%)	1 (<1%)	43 (21%)
Phantom	**16cm**	205	0	58 (29%)
	32cm	0	196	142 (71%)
CTDI	**AIDR active (mGy, median, 95% CI for the mean)**	22,1 (21,6-23,3)	1,0 (1,3-1,7)	2,7 (3,3-4,7)
	No AIDR (mGy, median, 95% CI for the mean)	38,7 (36,1-39,5)	9,8 (-2,2-21,4)	4,8 (4,8-7,1)
DLP	**AIDR active (mGy.cm, median, 95% CI for the mean)**	365,1 (437,8-506,2)	27,3 (40,1-54,2)	93,1 (133,2-203,8)
	No AIDR (mGy.cm, median, 95% CI for the mean)	652,8 (591,3-877,5)	241,9 (4,6-452,5)	176,2 (174,8-280,7)
SSDE	**AIDR active (mGy, median, 95% CI for the mean)**	22,4 (22,2-23,8)	2,0 (2,3-2,7)	3,4 (4-5,2)
	No AIDR (mGy, median, 95% CI for the mean)	37,5 (35,1-38,5)	13,5 (-3,2-29,6)	8,7±6,0
Helical		106 (52%)	168 (86%)	178 (89%)
Volume		99 (48%)	28 (14%)	22 (11%)
AIDR active		185 (90%)	193 (99%)	131 (66%)
Scan length (cm, median, 95% CI for the mean)		160,0 (178,6-193,5)	228,0 (226,4-248,0)	346,3 (331,9-357,9)
Effective Diameter (cm, median, 95% CI for the mean)		15,5±1,3	19,4 (19,2-20,5)	20,0 (19,8-21,0)

Abbreviations

DLP: dose length product

AIDR: adaptative iterative dose reduction

CTDIVOL: computed tomography dose index

SSDE: size-specific dose estimates

CI: confidence interval

IMAGE NOISE ANALYSIS

HEAD EXAMINATIONS

Image noise was analyzed in native CT scans (n=182), subdivided according to tube voltage. Higher noise measurements can be seen in examinations with lower tube voltage. Five examinations were done with 80 kV. The most missing cases were seen in the lateral ventricle measurements (n=41), with a total of 58 (28%) missing cases in al head examinations. Table 12 and Figure 19 summarize the mean/median values for each ROI and Tables 13 to 15 show the number of missing cases per region and ROI.

Table 12. Noise Values (HU) per ROI according to kV in Native Head Examinations

	80 kV	100 kV	120 kV
Background Noise 1	2,7±0,9 ɤ	2,0 (2,0-2,5)*	1,4 (1,6-1,8)*
Background Noise 2	2,3±0,7ɤ	2,0 (1,9-2,4)*	1,4 (1,6-1,9)*
Centrum Semiovale 1	5,6 (2,6-9,8)*	3,9 (3,8-4,3)*	4,1 (4,0-4,3)*
Centrum Semiovale 2	5,1 (1,7-10,5)*	3,9 (3,8-4,2)*	4,1 (4,1-4,4)*
Lateral Ventricle 1	6,0 (1,6-11,0)*	4,7±1,0ɤ	4,6 (4,6-5,0)*
Lateral Ventricle 2	5,5 (1,7-11,3)*	4,5 (4,5-5,1)*	4,8±1,1ɤ
Cortex 1	5,8±3,2ɤ	4,2 (4,1-4,4)*	4,2 (4,2-4,5)*
Cortex 2	5,4 (2,5-9,2)*	4,3±0,7ɤ	4,4±0,7ɤ

ɤ Mean ± SD
* Median (95% Confidence Interval)

Figure 19. Noise Values (HU) per ROI according to kV in Native Head Examinations

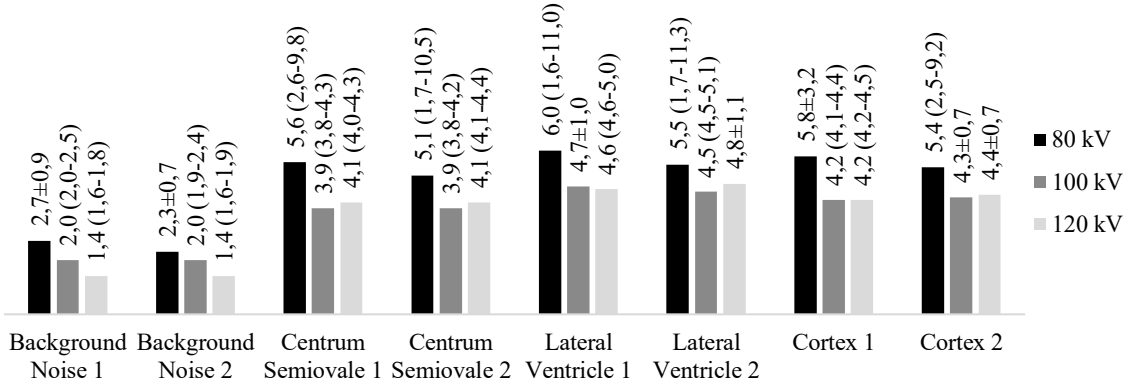

There were in total 23 head examinations with CM in the database. Mean noise image values are summarized in Table 13. No examinations with CM was done with a tube voltage of 80

kV. When graphed (Fig. 20), head examinations with CM at 100 kV showed slightly higher image noise mean values as those made with a 120 kV tube voltage.

Table 13. Noise Values (HU) per ROI according to kV in Head Examinations with CM

	100 kV	120 kV
Background Noise 1	3,2±1,4ɤ	2,1±0,7ɤ
Background Noise 2	3,1±1,2ɤ	1,2±0,6ɤ
Centrum Semiovale 1	5,5±1,1ɤ	4,8±0,9ɤ
Centrum Semiovale 2	5,3±1,0ɤ	4,9±0,8ɤ
Lateral Ventricle 1	5,9±1,3ɤ	6,0±1,4ɤ
Lateral Ventricle 2	6,2±1,2ɤ	6,1±1,9ɤ
Cortex 1	5,6±0,9ɤ	5,0±0,8ɤ
Cortex 2	5,6±0,9ɤ	5,2±0,8ɤ

ɤ Mean ± SD

Figure 20. Noise Values (HU) per ROI according to kV in Head Examinations with CM

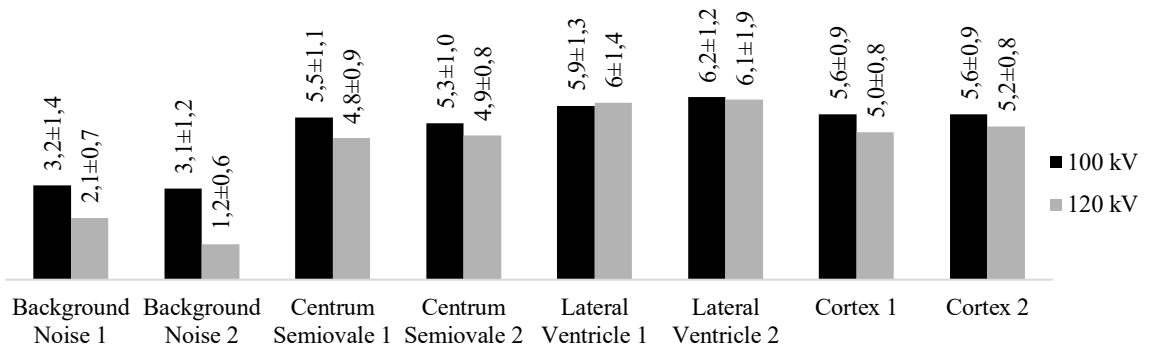

Furthermore, measurements in centrum semiovale were compared within native examinations grouped by tube voltage. Native examinations with an 80 kV tube voltage (n=5) had a significantly higher image noise as those with a 100 kV tube voltage (n=69) for both centrum semiovale ROI measurements. For comparison between 100 kV native examinations (n=69) and 120 kV native examinations (n=99), a statistically significant higher mean noise value was seen in both ROIs with a 120 kV tube voltage. The comparison between 80 kV and 120 kV native examinations showed a statistically significant higher mean noise values in centrum semiovale of 80 kV examinations. This was not the case for centrum semiovale ROI 2, were mean values showed no statistical difference between their mean values. P-values are summarized in Table 14.

Table 14. Image Noise Comparison according to Tube Voltage in Native Head Examinations			
	P-Value		
	80kV vs 100kV	80kV vs 120kV	100kV vs 120kV
Centrum Semiovale 1	0,020*+	0,027**+	0,013**+
Centrum Semiovale 2	0,045*+	0,084**+	0,004**+

* Exact Significance (2-sided test)
**Asymptotic Significance (2-sided test)
+Mann-Whitney U-test
Statistically significant p-values are underlined

When comparing mean noise values of both centrum semiovale ROI measurements between 100 kV native examinations (n=69) and 100 kV (n= 18) examinations with CM, P-value was <0,05 for both ROIs, showing statistically significant higher image noise in examinations with CM. On the contrary, the same comparison was made in 120 kV examinations (native n=99; CM n=5), where no statistically significant difference was found in image noise mean value. Exact P-values are summarized in Table 15.

Table 15. Image Noise Comparison according to Tube Voltage in Head Examinations		
	P-Value	
	Native 100 kV vs CM 100 kV	Native 120 kV vs CM 120 kV
Centrum Semiovale 1	0,000**+	0,051**+
Centrum Semiovale 2	0,000**+	0,089**+

**Asymptotic Significance (2-sided test)
+Mann-Whitney U-test
Statistically significant p-values are underlined

CHEST EXAMINATIONS

For native chest examinations (n=112), median and mean image noise values are summarized in Table 16 according to tube voltage. Higher image noise values in 80 kV examinations are seen in background noise ROIs and trachea ROI. Almost homogenous values can be seen for the aortic arch, and right heart ventricle ROIs and higher noise values are seen for examinations with 100 kV and 120 kV tube voltage in left heart ventricle and both paravertebral muscle ROIs. Figure 21 depicts these values. There was a total of 14 (7%) missing cases.

Table 16. Noise Values (HU) per ROI according to kV in Native Chest Examinations			
	80 kV	**100 kV**	**120 kV**
Background Noise 1	13,2 (10,5-16,0)*	10,6 (10,4-11,8)*	8,9 (8,8-10,2)*
Background Noise 2	10,9 (8,5-13,5)*	10,6 (10,4-12,7)*	9,4 (9,3-10,8)*
Trachea	18,7 (9,4-24,3)*	15,5 (15,1-17,5)*	14,7±2,8ɤ
Aortic Arch	14,3 (11,2-17,4)*	14,4±2,7 ɤ	13,8±2,6ɤ
Right Heart Ventricle	13,4 (8,4-16,1)*	14,1±2,2ɤ	14,1±2,1ɤ
Left Heart Ventricle	12,3 (11,0-14,3)*	14,2±2,1 ɤ	13,9 (13,7-14,6)*
Paravertebral Muscles 1	15,6 (9,8-21,1)*	17,9±3,5 ɤ	17,7±2,8ɤ
Paravertebral Muscles 2	13,4 (9,3-17,2)*	17,9±3,0ɤ	17,6±2,8ɤ

ɤ Mean ± SD
* Median (95% Confidence Interval)

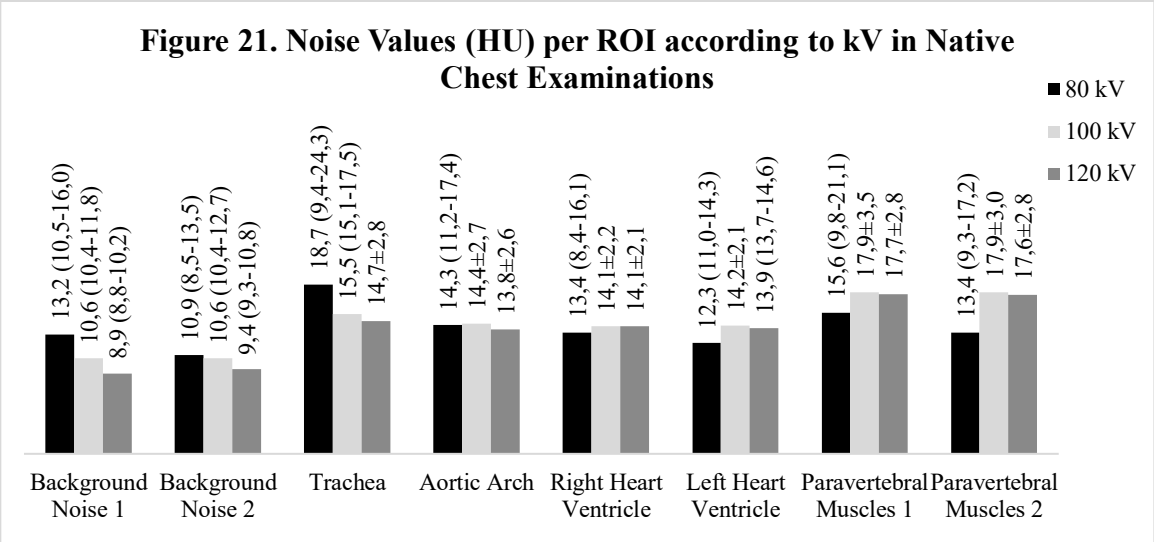

Image noise median and mean values for chest examinations with CM (n=84) are summarized in Table 17, according to tube voltage. Higher image noise values are seen in 80 kV examinations, except for the paravertebral muscle ROIs, where 120 kV examinations show higher image noise measurements. These data are better depicted in Figure 22.

Table 17. Noise Values (HU) per ROI according to kV in Chest Examinations with CM			
	80 kV	100 kV	120 kV
Background Noise 1	11,5±3,8ɤ	10,2±2,2ɤ	8,6±1,7ɤ
Background Noise 2	10,9 (8,5-14,2)*	10,4±2,2ɤ	9,2±1,6ɤ
Trachea	17,2±3,3ɤ	16,8±4,1ɤ	15,5 (14,5-17,2)*
Aortic Arch	19,4±5,6ɤ	15,1 (14,9-17,5)*	15,3±2,5ɤ
Right Heart Ventricle	20,8±7,3ɤ	16,2 (15,7-18,4)*	16,0 (15,5-19,8)*
Left Heart Ventricle	19,0±5,2ɤ	15,8 (15,2-19,6)*	17,1 (16,5-19,3)*
Paravertebral Muscles 1	16,0±3,4ɤ	15,9 (15,3-17,5)*	17,4±3,3ɤ
Paravertebral Muscles 2	13,3 (12,4-15,4)*	16,9±3,8ɤ	17,3±3,3ɤ

ɤ Mean ± SD
* Median (95% Confidence Interval)

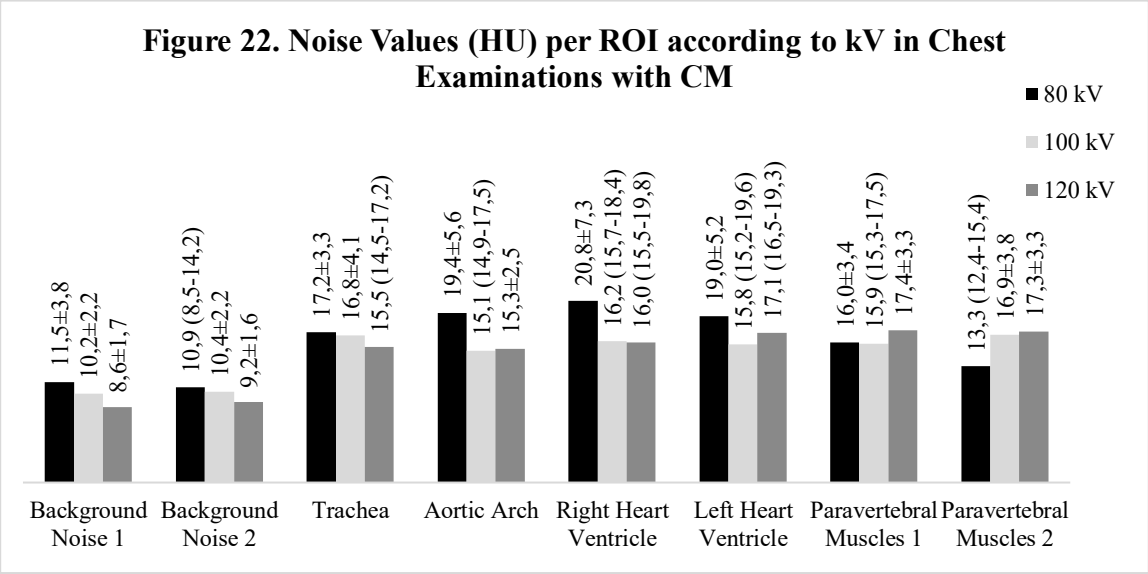

Image noise measurements in the aortic arch were compared in native chest examinations with 80 kV (n=2) and 100 kV (n=45). There was no statistically significant difference between their mean image noise values. The same result was found after comparing native chest CTs with 80 kV and 120 kV studies (n=63). However, a significant difference ($p < 0,05$) was found after comparing native chest CTs with 100 kV and 120 kV. Statistically, significant higher mean image noise values belonged to 100 kV studies. Exact p-values are summarized in Table 18.

Table 18. Image Noise Comparison according to Tube Voltage in Native Chest Examinations			
	P-Value		
	80kV vs 100kV	80kV vs 120kV	100kV vs 120kV
Aortic Arch	0,936*+	0,509*+	0,000µ

* Exact Significance (2-sided test)
+Mann-Whitney U-test
µ Independent Samples T-Test
Statistically significant p-values are underlined

When comparing for the same ROI between 80 kV native examinations and 80 kV (n=10) examinations with CM, no statistically significant difference was found. The same could be seen for the comparison between native 120 kV and 120 kV (n=35) with CM. However, p <0,05 showed a significantly higher mean image noise values for the 100 kV examinations (n=39) with CM when compared to 100 kV native examinations. Exact p-values are summarized in Table 19.

Table 19. Image Noise Comparison according to Tube Voltage in Chest Examinations			
	P-Value		
	Native 80kV vs CM 80 kV	Native 100kV vs CM 100 kV	Native 120kV vs CM 120 kV
Aortic Arch	0,273*+	0,032**+	0,880µ

**Asymptotic Significance (2-sided test)
+Mann-Whitney U-test
µ Independent Samples T-Test
Statistically significant p-values are underlined

ABDOMINAL EXAMINATIONS

Mean image noise values for native abdominal examinations (n=178) are summarized in Table 20 according to tube voltage. Higher values are seen in 120 kV tube voltage examinations. There were no 80 kV examinations for native studies to analyze. This increase in noise is better depicted in Figure 23. There was a total of 20 (10%) missing cases.

Table 20. Noise Values (HU) per ROI according to kV in Native Abdominal Examinations		
	100 kV	120 kV
Background Noise 1	7,6±1,3ɣ	10,4±3,2ɣ
Background Noise 2	7,6±1,3ɣ	9,1±2,4ɣ
Spleen	13,3±3,4ɣ	13,9±2,9ɣ
Gallbladder	11,7±3,0ɣ	14,1±2,1ɣ
Liver 1	12,6±2,8ɣ	14,9±2,6ɣ
Liver 2	11,3±2,3ɣ	13,7±3,0ɣ

Psoas Muscle 1	13,8±2,9ɤ	16,3±4,9ɤ
Psoas Muscle 2	13,4±2,8ɤ	15,5±2,2ɤ

ɤ Mean ± SD

Figure 23. Noise Values (HU) per ROI according to kV in Native Abdominal Examinations

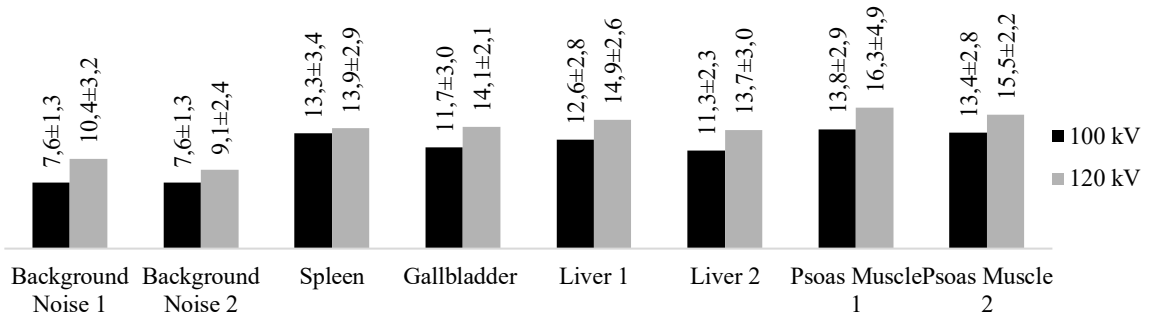

In contrast, mean image noise values were higher for studies with lower tube voltage in examinations with CM (n=178). An exception is seen for psoas muscle ROI 1, where the mean values seen in 80 kV and 120 kV are similar. Mean and median image noise values are summarized in Table 21 and presented as a graphic in Figure 24.

Table 21. Noise Values (HU) per ROI according to kV in Abdominal Examinations with CM

	80 kV	100 kV	120 kV
Background Noise 1	9,9±2,8ɤ	8,9 (8,5-9,5)*	8,6 (8,4-9,4)*
Background Noise 2	9,1±2,9ɤ	8,9±2,0ɤ	8,3 (8,3-9,3)*
Spleen	15,4 (12,5-21,4)*	13,3 (13,9-15,6)*	13,3 (13,1-14,4)*
Gallbladder	15,2±4,8ɤ	12,5 (12,2-14,7)*	12,4±3,22ɤ
Liver 1	15,8±5,0ɤ	13,3 (13,3-14,6)*	13,8 (13,5-14,7)*
Liver 2	15,3±4,9ɤ	13,0±2,7ɤ	12,7±2,3ɤ
Psoas Muscle 1	15,6 (12,9-20,9)*	14,1 (14,0-15,5)*	15,1±3,4ɤ
Psoas Muscle 2	16,5±4,6ɤ	14,6±3,1ɤ	13,9 (13,6-15,1)*

ɤ Mean ± SD
* Median (95% Confidence Interval)

Figure 24. Noise Values (HU) per ROI according to kV in Abdominal Examinations with CM

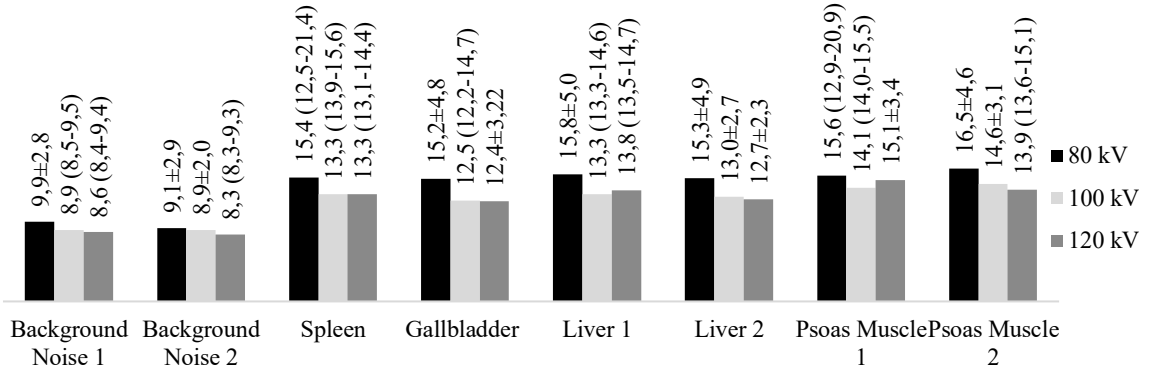

When comparing image noise mean values between native studies with 100 kV (n=10) and 120 kV (n=12) for both liver ROIs, 120 kV studies form liver ROI 1 had statistically significant higher values. For liver ROI 2, no statistically significant difference was found. P-values for this test are summarized in Table 22. No native examinations were made at an 80 kV tube voltage.

Table 22. Image Noise Comparison according to Tube Voltage in Native Abdominal Examinations

	P-Value
	100kV vs 120kV
Liver 1	0,012$^{\mu}$
Liver 2	0,450$^{\mu}$

µ Independent Samples T-Test
Statistically significant p-values are underlined

No statistically significant difference was found in the mean image noise values between native studies and studies with CM in both liver ROIs at both 100 kV and 120 kV. P-values for this test are summarized in Table 23.

Table 23. Image Noise Comparison according to Tube Voltage in Abdominal Examinations

	P-Value	
	Native 100kV vs CM 100 kV	**Native 120kV vs CM 120 kV**
Liver 1	0,243^{**+}	0,324^{**+}
Liver 2	0,577$^{\mu}$	0,108$^{\mu}$

**Asymptotic Significance (2-sided test)
+Mann-Whitney U-test
µ Independent Samples T-Test

SUBJECTIVE DATA ANALYSIS

Overall data were analyzed according to the described subjective scale in the methods and materials section. In Table 24, the frequency of examinations per region was summarized according to the subjective noise analysis. It was subdivided into native examinations and examinations with CM. Head examinations have better subjective image scores when compared to the chest and abdominal regions. Abdominal examinations show mostly a "moderate" image noise. On the contrary, in chest examinations, image noise tends to be higher.

Table 24. Percentage of Examinations according to Subjective Noise Analysis and CM per Region

		Minimal	Low	Moderate	Significant Noise	Excessive Noise
Head	CM + (n=23)	3 (13%)	6 (26%)	10 (44%)	4 (17%)	-
	CM – (n=182)	110 (61%)	49 (27%)	15 (8%)	6 (3%)	2 (1%)
Chest	CM + (n=84)	-	-	11 (13%)	47 (56%)	26 (31%)
	CM – (n=112)	-	1 (1%)	21 (19%)	72 (64%)	18 (16%)
Abdomen	CM + (n=178)	2 (1%)	4 (2%)	119 (67%)	34 (19%)	19 (11%)
	CM – (n=22)	-	-	14 (64%)	6 (27%)	2 (9%)

Table 25 summarizes the frequency of studies according to the subjective analysis of overall image quality. Head examinations obtained mostly "optimal" subjective grading, while chest and abdominal examinations mostly "acceptable". "Unacceptable" examinations were more frequent in the abdominal area, with a total of nine studies. Head examinations had the least, with two and chest examinations three.

Table 25. Percentage of Examinations according to Subjective Analysis of Overall Image Quality and CM per Region

		Optimal	**Acceptable**	**Unacceptable**
Head	CM + (n=23)	21 (91%)	2 (9%)	-
	CM – (n=182)	167 (92%)	13 (7%)	2 (1%)
Chest	CM + (n=84)	18 (22%)	65 (77%)	1 (1%)
	CM – (n=112)	11 (10%)	99 (88%)	2 (2%)
Abdomen	CM + (n=178)	21 (12%)	150 (84%)	7 (4%)
	CM – (n=22)	2 (9%)	18 (82%)	2 (9%)

NATIVE HEAD EXAMINATIONS

Native head examinations were 182 in total. From these, 110 examinations obtained a "minimal" subjective noise grading (Table 24). When comparing to image noise measurements in each ROI (Table 26), lowest mean values were obtained in the "minimal" grading.

Higher noise values are seen in higher categories of the subjective noise analysis scale. Six native examinations figured in the "significant noise" grading, while just two examinations were graded as with "excessive noise". In examinations with "excessive noise", cortex ROIs could not be well-differentiated due to high noise levels.

Table 26. Noise Values (HU) per ROI according to Subjective Noise Analysis in Native Head Examinations

	Minimal n=110	Low n=49	Moderate n=15	Significant Noise n=6	Excessive Noise n=2
Background Noise 1	1,7 (1,6-1,8)*	2,0 (2,0-2,4)*	2,3±0,7ɤ	2,4±0,8ɤ	6,4 (-20,9-33,7)*
Background Noise 2	1,6 (1,6-1,9)*	2,0 (1,8-2,3)*	2,2±0,8ɤ	2,1±1,1ɤ	5,2 (-16,9-27,2)*
Centrum Semiovale 1	3,9 (3,7-3,9)*	4,4±0,6ɤ	5,0±0,6ɤ	5,9 (4,8-7,1)*	11,0 (10,1-11,9)*
Centrum Semiovale 2	3,8±0,5ɤ	4,4±0,7ɤ	4,9±0,5ɤ	5,8±0,7ɤ	11,2 (-0,5-22,8)*
Lateral Ventricle 1	4,4±0,9ɤ	5,0±0,8ɤ	5,4±0,9ɤ	6,5±1,5ɤ	10,3 (-18,1-38,7)*
Lateral Ventricle 2	4,5±1,0ɤ	5,0±1,1ɤ	5,6±0,7ɤ	5,3 (4,9-6,5)*	11,0 (-17,1-39,1)*
Cortex 1	4,0±0,5ɤ	4,6±0,5ɤ	5,1±0,6ɤ	6,1±0,6ɤ	-
Cortex 2	4,0±0,5ɤ	4,6 (4,4-4,7)*	5,4±0,6ɤ	5,9±0,8ɤ	-

ɤ Mean ± SD
* Median (95% Confidence Interval)

Regarding the subjective analysis of overall image quality, 92% (n=167) of native head examinations were graded as "optimal" (Table 25). From these, 110 were categorized in the "minimal" subjective noise. The other 57 were rated with "low" and "moderate" noise. Thirteen native examinations were graded as "acceptable", seven categorized as "moderate" and six as "significant noise" in the subjective noise scale. The two head native examinations which obtained an "unacceptable" subjective overall image quality grading were also those who had "excessive noise" grading and highest median image noise values. Image noise measurements are summarized in Table 27, according to the subjective overall image quality scale.

Table 27. Noise Values (HU) per ROI according to Subjective Analysis of Overall Image Quality in Native Head Examinations			
	Optimal n=167	Acceptable n=13	Unacceptable n=2
Background Noise 1	1,7 (1,8-2,0)*	2,1±0,8ɤ	6,4 (-20,9-33,7)*
Background Noise 2	1,7 (1,7-2,0)*	2,0±0,9ɤ	5,2 (-16,9-27,2)*
Centrum Semiovale 1	4,0 (3,9-4,1)*	5,3±0,8ɤ	11 (10,1-11,9)*
Centrum Semiovale 2	4,0 (3,9-4,1)*	5,5±0,6ɤ	11,2 (-0,5-22,8)*
Lateral Ventricle 1	4,6 (4,5-4,8)*	5,9±1,3ɤ	10,3 (-18,1-38,7)*
Lateral Ventricle 2	4,7±1,1ɤ	5,9±0,7ɤ	11 (-17,1-39,1)*
Cortex 1	4,1 (4,2-4,3)*	5,5±0,9ɤ	-
Cortex 2	4,2 (4,2-4,3)*	5,4 (5,2-6,0)*	-

ɤ Mean ± SD
* Median (95% Confidence Interval)

HEAD EXAMINATIONS WITH CM

A total of 23 head examinations were done with a contrast agent. 44% (n=10) of them were rated as “moderate” in the subjective noise analysis scale. No examination had an “excessive noise” grading, but four were graded as “significant noise” (Table 24).

The comparison of subjective image noise analysis with image noise measurements in different regions is illustrated in Table 28. An increase in image noise is observed as the subjective grading increases.

Table 28. Noise Values (HU) per ROI according to Subjective Noise Analysis in Head Examinations with CM				
	Minimal n=3	Low n=6	Moderate n=10	Significant Noise n=4
Background Noise 1	1,4 (-1,4-6,0)*	2,8±1,5ɤ	2,9±0,8ɤ	3,4 (0,7-6,9)*
Background Noise 2	2,0 (-0,4-5,4)*	2,9±1,7ɤ	2,7±0,9ɤ	3,6 (1,5-5,1)*
Centrum Semiovale 1	3,7 (2,2-5,8)*	4,7±0,6ɤ	5,8±0,8ɤ	6,4 (4,4-8,1)*
Centrum Semiovale 2	4,0 (2,4-5,5)*	4,5±0,7ɤ	5,7±0,7ɤ	6,2 (5,0-7,2)*
Lateral Ventricle 1	4,4 (2,5-6,8)*	4,7±1,3ɤ	6,3±1,1ɤ	6,4 (4,6-8,7)*
Lateral Ventricle 2	4,9 (3,6-6,4)*	5,0±1,0ɤ	7,0±1,1ɤ	6,9 (4,5-8,3)*
Cortex 1	5,0 (3,5-6,5)*	4,8±0,7ɤ	5,9±0,8ɤ	5,6 (3,9-7,2)*
Cortex 2	5,0 (3,0-6,9)*	4,7±0,4ɤ	5,9±0,5ɤ	6,6 (4,6-8,5)*

ɤ Mean ± SD
* Median (95% Confidence Interval)

In the subjective analysis of overall image quality, 21 examinations with a contrast agent were classified as “optimal” and just two as “acceptable” (Table 25). These two examinations were graded with “significant noise” in the subjective noise scale. Two of the “optimal” examinations were also graded with “significant noise”.

Table 29 shows image noise measurements according to the subjective analysis of overall image quality. Higher noise levels can be found in the “acceptable” category. Image noise levels are similar within both categories with an increasing trend of image noise in the “acceptable” category.

Table 29. Noise Values (HU) per ROI according to Subjective Analysis of Overall Image Quality in Head Examinations with CM

	Optimal n=21	Acceptable n=2
Background Noise 1	2,8±1,1ɤ	4,3 (-24,7-33,3)*
Background Noise 2	2,8±1,2ɤ	2,9 (-12,3-18,1)*
Centrum Semiovale 1	5,4±1,1ɤ	5,4 (-2,2-13,0)*
Centrum Semiovale 2	5,2±1ɤ	5,6 (0,5-10,7)*
Lateral Ventricle 1	5,9±1,4ɤ	5,8 (3,1-8,5)*
Lateral Ventricle 2	6,1±1,4ɤ	6,9 (3,2-10,6)*
Cortex 1	5,5±0,9ɤ	4,7 (3,3-6,1)*
Cortex 2	5,6±1,0ɤ	5,4 (0,1-10,7)*

ɤ Mean ± SD
* Median (95% Confidence Interval)

NATIVE CHEST EXAMINATIONS

64% (n=72) of the native chest CTs (n=112) were graded with “significant noise”. Just one examination obtained “low” subjective image noise grading and 18 obtained “excessive noise” grading (Table 24).

Table 30. Noise Values (HU) per ROI according to Subjective Noise Analysis in Native Chest Examinations

	Low n=1	Moderate n=21	Significant Noise n=72	Excessive Noise n=18
Background Noise 1	6,4	8,9±1,4ɤ	9,7 (9,6-11,0)*	12,0±2,4ɤ
Background Noise 2	5,1	9,9±1,6ɤ	9,8 (9,8-11,6)*	11,7±2,6ɤ
Trachea	16,2	14,3±2,1ɤ	15,1 (14,6-16,3)*	16,5±3,3ɤ
Aortic Arch	8,7	13,4±1,5ɤ	13,6±2,1ɤ	17,2±3,5ɤ
Right Heart Ventricle	11,14	12,9±1,3ɤ	13,6 (13,6-14,5)*	15,6±3,2ɤ

Left Heart Ventricle	11,14	13,0 (12,9-14,0)*	13,9 (13,7-14,5)*	15,2±2,9ɤ
Paravertebral Muscles 1	17,4	16,7±2,5ɤ	17,8±3,3ɤ	18,7±3,1ɤ
Paravertebral Muscles 2	15,7	16,5±2,7ɤ	17,3 (17,1-18,4)*	18,3±4,0ɤ

ɤ Mean ± SD
* Median (95% Confidence Interval)

Table 30 summarizes image noise measurements according to subjective noise analysis. Since there was only one examination with "low" subjective noise, descriptive statistics could not be calculated. Most of the native chest examinations fell into the "acceptable" category of subjective overall image quality. In contrast, just two examinations rated as "optimal" and 11 as "unacceptable" (Table 25).

Mean noise values classified according to subjective overall image quality are summarized in Table 31. It shows homogenous values throughout the three classifications and ROIs, except for the background noise ROIs, where image noise measurements increase substantially at the "unacceptable category". Furthermore, noise tends also to decrease slightly in paravertebral muscle ROIs.

Table 31. Noise Values (HU) per ROI according to Subjective Analysis of Overall Image Quality in Native Chest Examinations

	Optimal n=11	Acceptable n=99	Unacceptable n=2
Background Noise 1	9,6±2,3ɤ	9,7 (9,7-10,9)*	13,8 (1,2-26,4)*
Background Noise 2	9,9±3,2ɤ	10,1 (10,0-11,3)*	15,9 (3,2-28,7)*
Trachea	15,4±2,1ɤ	15,0 (14,6-15,9)*	22,8 (-20,1-65,6)*
Aortic Arch	13,7±2,3ɤ	13,9 (13,6-14,6)*	14,4 (-9,3-38,1)*
Right Heart Ventricle	14,3±2,3ɤ	13,5 (13,5-14,4)*	15,3 (-19,8-50,4)*
Left Heart Ventricle	14,4±2,7ɤ	13,9 (13,7-14,4)*	15,0 (-25,3-55,3)*
Paravertebral Muscles 1	17,5±2,8ɤ	17,7±3,2ɤ	17,3 (-32,1-66,7)*
Paravertebral Muscles 2	18,3±3,1ɤ	17,5±3,0ɤ	16,3 (14,1-18,6)*

ɤ Mean ± SD
* Median (95% Confidence Interval)

CHEST EXAMINATIONS WITH CM

From the 84 chest examinations, with contrast agent, 56% (n=47) were graded with "significant noise", according to the subjective noise analysis. 31% (n=26) had "excessive noise", and 11 examinations presented a "moderate" rating (Table 24).

Image noise mean and median values were documented in Table 32 according to image noise analysis. For each ROI, values increased according to the category of subjective noise.

Table 32. Noise Values (HU) per ROI according to Subjective Noise Analysis in Chest Examinations with CM

	Moderate n=11	Significant Noise n=47	Excessive Noise n=26
Background Noise 1	8,6±1,7ɤ	9,5±2,1ɤ	10,4±3,1ɤ
Background Noise 2	9,3±2,2ɤ	9,5 (9,3-10,3)*	10,3 (9,3-12,0)*
Trachea	14,6±3,0ɤ	16,1±3,1ɤ	17,9±5,2ɤ
Aortic Arch	13,8±1,2ɤ	15,0 (14,4-16,1)*	18,4 (17,0-20,8)*
Right Heart Ventricle	15,6±1,8ɤ	15,7 (15,4-18,1)*	18,6 (17,4-23,5)*
Left Heart Ventricle	14,9±2,4ɤ	16,3 (15,6-19,2)*	19,7±5,0ɤ
Paravertebral Muscles 1	15,7±2,3ɤ	16,3 (14,1-17,2)*	16,9±3,2ɤ
Paravertebral Muscles 2	16,0±2,7ɤ	16,7±3,3ɤ	17,2±4,3ɤ

ɤ Mean ± SD
* Median (95% Confidence Interval)

77% (n=65) of the examinations were classified as "acceptable" in the subjective analysis of overall image quality. In contrast, just one examination was graded as "unacceptable". The remaining 18 examinations were classified as "optimal" (Table 25).

Image noise measurements according to overall image quality are summarized in Table 33. Image noise was higher in aortic arch, left heart ventricle, and paravertrebral muscles in the "optimal" grading category.

Table 33. Noise Values (HU) per ROI according to Subjective Analysis of Overall Image Quality in Chest Examinations with CM

	Optimal n=18	Acceptable n=65	Unacceptable n=1
Background Noise 1	8,8±1,7ɤ	9,5 (9,3-10,6)*	7,6
Background Noise 2	9,5±2,2ɤ	9,6 (9,5-10,8)*	10,7
Trachea	14,6±2,2ɤ	16,7±3,6ɤ	34,2
Aortic Arch	15,6±2,5ɤ	15,1 (15,2-17,3)*	19,7
Right Heart Ventricle	15,7 (14,1-21,8)*	16,3 (16,4-18,8)*	22,3
Left Heart Ventricle	17,2±3,1ɤ	17,0 (16,4-19,4)*	19,8
Paravertebral Muscles 1	16,4±2,9ɤ	16,2 (16,0-17,8)*	-

Paravertebral Muscles 2	17,4±3,7ɤ	16,6±3,5ɤ	-

ɤ Mean ± SD
* Median (95% Confidence Interval)

NATIVE ABDOMINAL EXAMINATIONS

From the 22 native abdominal examinations, 14 were classified with "moderate" subjective noise. Two examinations were graded with "excessive noise", and six with significant noise (Table 24). Image noise measurements according subjective noise analysis are summarized in Table 34.

Table 34. Noise Values (HU) per ROI according to Subjective Noise Analysis in Native Abdominal Examinations

	Moderate n=14	Significant Noise n=6	Excessive Noise n=2
Background Noise 1	8,1 (7,0-9,6)*	9,9±2,9ɤ	12,8 (-32,5-58,1)*
Background Noise 2	7,6±1,6ɤ	9,7±2,6ɤ	10,1 (-7,5-27,7)*
Spleen	12,3±2,1ɤ	16,2±2,9ɤ	15,2 (-32,7-63,2)*
Gallbladder	12,3±2,7ɤ	13,4±3,1ɤ	14,4 (-20,6-49,3)*
Liver 1	12,4±2,2ɤ	16,4±2,1ɤ	16,3 (-13,5-46,1)*
Liver 2	11,3±1,8ɤ	14,5±3,4ɤ	16,1 (-1,8-34,0)*
Psoas Muscle 1	13,5 (11,6-17,0)*	15,2±3,2ɤ	18,8 (15,5-22,0)*
Psoas Muscle 2	13,8±2,3ɤ	15,5±3,1ɤ	17,6 (16,3-18,9)*

ɤ Mean ± SD
* Median (95% Confidence Interval)

Most native abdominal examinations (n=18; 82%) were graded as "acceptable" according to the subjective overall image quality scale. Two examinations were graded respectively as "optimal" and "unacceptable" (Table 25). Image noise measurements were higher in acceptable and unacceptable categories (Table 35).

Table 35. Noise Values (HU) per ROI according to Subjective Analysis of Overall Image Quality in Native Abdominal Examinations

	Optimal n=2	Acceptable n=18	Unacceptable n=2
Background Noise 1	7,7 (-4,2-19,7)*	8,5 (7,6-10,4)*	11,9 (-21,7-45,5)*
Background Noise 2	6,9 (-6,1-19,8)*	8,4±2,1ɤ	10,3 (-9,7-30,3)*
Spleen	13,1 (-5,7-31,8)*	13,6 (12,0-15,1)*	14,9 (-28,6-58,4)*
Gallbladder	10,5 (-3,2-24,2)*	12,9±2,8ɤ	14,3 (-19,2-47,7)*
Liver 1	10,3 (5,1-15,5)*	14,1±2,8ɤ	15,6 (-4,9-36,0)*

Liver 2	10,7 (-16,9-38,3)*	12,4±2,7ɤ	16,5 (-5,7-38,6)*
Psoas Muscle 1	12,5 (-8,8-33,8)*	15,0±4,4ɤ	19,1 (18,2-20,1)*
Psoas Muscle 2	12,1 (-9,9-34,2)*	14,5±2,3ɤ	17,5 (17,2-17,8)*

ɤ Mean ± SD
* Median (95% Confidence Interval)

ABDOMINAL EXAMINATIONS WITH CM

One hundred seventy-eight abdominal examinations were used with the aid of a contrast agent. From these, 119 were classified as "moderate" according to the subjective noise analysis. Two examinations were classified as "minimal" subjective noise, whereas 19 examinations were graded with "excessive noise" (Table 24).

Image noise values are summarized in Table 36 according to the subjective noise analysis scale. Higher noise measurements are seen in classifications such as "significant noise" and excessive noise.

Table 36. Noise Values (HU) per ROI according to Subjective Noise Analysis in Abdominal Examinations with CM

	Minimal n=2	Low n=4	Moderate n=119	Significant Noise n=34	Excessive Noise n=19
Background Noise 1	5,2 (-11,9-22,3)*	5,3 (5,1-5,7)*	8,6±1,7ɤ	9,8±2,6ɤ	10,7±2,8ɤ
Background Noise 2	5,6 (-19,0-30,1)*	5,5 (4,1-6,8)*	8,3 (8,1-8,8)*	9,8±2,3ɤ	10,0±2,6ɤ
Spleen	7,9 (-15,4-31,2)*	10,4 (6,6-12,7)*	12,9 (12,9-13,6)*	16,9 (15,1-17,4)*	19,9±5,6ɤ
Gallbladder	9,0 (-16,9-34,8)*	9,3 (5,3-11,4)*	12,1 (11,8-12,7)*	14,1±2,7ɤ	16,9 (14,2-25,6)*
Liver 1	7,0 (-1,1-15,2)*	8,9 (7,1-11,5)*	13,2±1,7ɤ	15,7±3,0ɤ	18,3±4,9ɤ
Liver 2	8,6 (-11,3-28,5)*	9,7 (8,4-11,0)*	12,2±1,6ɤ	14,3±2,6ɤ	17,5±3,5ɤ
Psoas Muscle 1	9,9 (-26,5-46,4)*	11,9 (6,7-15,2)*	13,9 (13,7-14,6)*	16,5±3,6ɤ	19,2±5,6ɤ
Psoas Muscle 2	10,1 (-26,2-46,3)*	9,9 (6,6-12,3)*	13,4 (13,2-13,9)*	16,4 (15,8-18,2)*	18,2±4,2ɤ

ɤ Mean ± SD
* Median (95% Confidence Interval)

Regarding the subjective analysis of overall image quality, 150 examinations were graded as "acceptable", 21 as "optimal" and seven as "unacceptable" (Table 25). Image noise

measurements were higher in “acceptable” and “unacceptable” categories, as seen in Table 37.

Table 37. Noise Values (HU) per ROI according to Subjective Analysis of Overall Image Quality in Abdominal Examinations with CM

	Optimal n=21	Acceptable n=150	Unacceptable n=7
Background Noise 1	7,5±2,2ɤ	9,0 (8,7-9,4)*	9,6±2,7ɤ
Background Noise 2	7,1±2,1ɤ	8,7 (8,6-9,3)*	9,7±3,6ɤ
Spleen	11,8±2,7ɤ	13,4 (10,6-13,0)*	17,8±4,7ɤ
Gallbladder	10,8±2,2ɤ	12,7 (12,7-14,3)*	13,5 (9,3-18,9)*
Liver 1	11,3 (9,9-12,2)*	13,7 (14,0-14,9)*	14,0 (11,7-19,2)*
Liver 2	10,6±1,6ɤ	12,8 (12,8-13,6)*	16,2±4,0ɤ
Psoas Muscle 1	13,0±2,7ɤ	14,4 (14,6-15,7)*	18,8±5,8ɤ
Psoas Muscle 2	12,0±2,3ɤ	14,1 (14,3-15,3)*	17,8±4,8ɤ

ɤ Mean ± SD
* Median (95% Confidence Interval)

DISCUSSION

This study aimed to provide clinically acceptable pediatric image noise ranges that could be applied in future scanning protocols. The provided data is specific for body region as well as for different anatomical structures and was analyzed according to age groups, tube voltage and CM. All included CT scans were considered diagnostic.

Ensuring the lowest risk to children while creating a diagnostic CT technique means accepting some degree of image noise to lower radiation[56]. Due to advances in CT technology, obtaining a good image quality is not an issue, but rather keeping radiation dose at its lowest and producing an appropriate image quality. CT scanning protocols and radiation dose guidelines exist nationwide and Europewide. Considering image noise levels in these protocols and tailoring protocols not only by age, size and weight, could bring CT further in terms of radiation dose optimization.

Of course, the diagnostic question plays an important role in the equation. Image noise is highly dependent on CM and applied parameters such as tube voltage and slice thickness. Lower tube voltage and slice thickness are inversely proportionate to image noise. However, with lower tube voltage, CM increases the examinations' contrast [57]. This allows higher image noise. Likewise, it could be of great importance to link image noise and the diagnostic information. The underlying pathology affects the chosen slice thickness and the use of CM. The examined tissue also changes the acceptance of image noise (e.g. bone tissue).

In this study, higher tube voltages were observed in older patients while lower tube voltages were more frequent in younger patients. This correlated with higher radiation dose estimates in older age groups, although in this study no statistical analysis on radiation dose was conducted. Regarding image noise analysis, native head examinations at 100 kV showed the lowest image noise values (for chosen ROI; $p<0,05$). Native chest examinations with 100 kV showed significantly higher image noise as examinations performed at 120 kV. Nonetheless, when comparing native and enhanced CT scans, higher image noise was seen in CM examinations, for both head and chest regions. For the abdominal examinations, no homogenous result was obtained, therefore, no tendency was found.

A high percentage of native head examinations obtained low scores in the subjective noise analysis and 92% were graded as "optimal". Chest and abdominal examinations were mostly rated as "acceptable" with a tendency to higher subjective image noise scores.

ROIs were chosen for each anatomical region based upon the most representative structures that provided a varied tissue density. Comparable studies show different ROI placing with a similar pattern when choosing structures within each region [46, 58, 67, 59–66]. Image noise in head CTs is most commonly measured in the white and gray matter, without choosing specific ROI locations. Resembling research studies of chest CTs measure image noise mainly on cardiac structures, with no specific ROI placement. There is more literature about image noise in the abdominal region, and ROIs tend to be placed in similar anatomical structures as our study. Through this study's results, we intend to create a precedent establishing image noise values for specific ROIs in specific anatomical regions.

Numerous studies focused on image noise as a primary determinant of image quality [46, 68, 69]. Studies like Liu et al. (pediatric study)[60] and Kilic et al. (adult study)[70] obtained similar mean noise values in similar ROIs of native head CTs with 120 kV and IR [60, 70], which is comparable to our image noise values at 120 kV. Scanning protocols in pediatric head CT with tube voltage under 120 kV are still not the trend[71–73], but our results support the possibility of implementing 100 kV tube voltage as an alternative, especially in younger pediatric patients (<10 years of age).

It was challenging to find comparison data to our results of the chest region. One study shows similar image noise measurements in the thoracic aorta (comparable to our aortic arch measurements) at two different 100 kV protocols[63]. This is one of the few studies that explore the integration of specific image noise measurements in predetermined ROIs for the development of CT scanning protocols. Enhanced examinations with low tube voltage, as well as the resulting values of image noise in the chest region are approached in the studies of Nagayama et al. and Sun et al[57, 58]. Our results reinforce their data and support the development of scanning protocols with radiation dose reduction in enhanced CT scans.

Studies like those of O' Connor et al. and Brisse et al[46, 74] had similar aims but produced lower image noise values in the enhanced abdominal CT with 100 kV, as compared to the ones in this study.

Although scanning protocols vary between ours and similar studies, these results are encouraging to produce clinically acceptable image noise values that contribute to the development of CT scanning algorithms and protocols.

LIMITATIONS

This study had several limitations. First, mAs could not be included due to the retrospective nature of this study and the automated exposure control (AEC) used in some of the examinations in the selected sample.

Another limitation was the lower population density in younger age groups. CT scan is avoided in younger patients, unless necessary, which explains this matter. Furthermore, weight and size were not this study's aims, nonetheless, an important variable to include when producing feasible scanning protocols.

This study focused mainly on the quantitative and qualitative criteria of the image quality in the examinations, not considering underlying pathology. Nonetheless, pathology could be relevant for image noise analysis in further attempts to revisit this research's topic.

Examinations at 80 kV were not the trend in the selected database, which also impairs its analysis and therefore, its ability to produce feasible data. It may be worth to explore this variable to create image noise data for younger patients.

The lead researcher is not an experienced radiologist. Paolicchi et al. proved that trained personnel can identify an acceptable image quality with diagnostic value and therefore, when properly trained in this matter, reduce the unnecessary usage of high tube voltages[71]. The "unacceptable" categorized examinations in this study had, for trained radiologists, a diagnostic value. Nonetheless, they just represented 2% of the 601 examinations.

CONCLUSION

Ensuring a diagnostic image quality with low radiation dose is not a new topic. However, establishing image noise ranges within different anatomical regions could be the next factor in the adjustment of CT protocols beside patient weight and size. This study expects to awake further interest and research on this topic and to highlight the need of region-specific image noise.

REFERENCES

[1] Damilakis J, Jarvinen H, Vock P, et al. *European Guidelines on DRLs for Paediatric Imaging*. 2016. Epub ahead of print 2016. DOI: 10.1594/esi2016/ESI-0011.

[2] Wachabauer D, Röthlin F. *Aktualisierung der diagnostischen Referenzwerte für Österreich*. Wien, https://jasmin.goeg.at/384/1/Aktualisierung der diagnostischen Referenzwerte_0-Fehler.pdf (2017).

[3] Brenner DJ, Hall EJ. Computed tomography - An increasing source of radiation exposure. *N Engl J Med* 2007; 357: 2277–2284.

[4] Tilla JE, Beck HL, Grogan HA, et al. A review of dosimetry used in epidemiological studies considered to evaluate the linear no-threshold (Lnt) dose-response model for radiation protection. *International Journal of Radiation Biology*. Epub ahead of print 2017. DOI: 10.1080/09553002.2017.1337280.

[5] Tack D, Gevenois PA. *Radiation Dose from Adult and Pediatric Multidetector Computed Tomography*. Berlin, Heidelberg, New York: Springer, 2007. Epub ahead of print 2007. DOI: https://doi.org/10.1007/978-3-540-68575-3.

[6] Mini RL, Vock P, Mury R, et al. Radiation exposure of patients who undergo CT of the trunk. *Radiology*. Epub ahead of print 1995. DOI: 10.1148/radiology.195.2.7724783.

[7] Van der Bruggen-Bogaarts BAHA, Broerse JJ, Lammers JWJ, et al. Radiation exposure in standard and high-resolution chest CT scans. *Chest*. Epub ahead of print 1995. DOI: 10.1378/chest.107.1.113.

[8] Kalender WA. Dose in x-ray computed tomography. *Phys Med Biol*; 59. Epub ahead of print 2014. DOI: 10.1088/0031-9155/59/3/R129.

[9] Sorantin E, Weissensteiner S, Hasenburger G, et al. CT in children-dose protection and general considerations when planning a CT in a child. *Eur J Radiol* 2013; 82: 1043–1049.

[10] Lubin JH, Adams MJ, Shore R, et al. Thyroid cancer following childhood low-dose radiation exposure: A pooled analysis of nine cohorts. *J Clin Endocrinol Metab*. Epub ahead of print 2017. DOI: 10.1210/jc.2016-3529.

[11] Brenner DJ, Elliston CD, Hall EJ, et al. Estimated Risks of Radiation-Induced Fatal Cancer from Pediatric CT. *Am Roentgen Ray Soc* 2001; 176: 289–296.

[12] Yu L, Bruesewitz MR, Thomas KB, et al. Optimal tube potential for radiation dose

reduction in pediatric CT: Principles, clinical implementations, and pitfalls. *RadioGraphics* 2011; 31: 835–848.

[13] Karami V, Gholami M, Lorestani S. Addressing as Low as Reasonably Achievable (ALARA) in Pediatric Computed Tomography (CT) Procedures. *J Res Med Dent Sci* 2018; 6: 104–114.

[14] van Gelderen F, van Gelderen F. A Brief History of Radiology. In: *Understanding X-Rays*. Springer Berlin Heidelberg, 2004, pp. 597–602.

[15] Kalender WA. *Computer Tomography. Fundamentals, System Technology, Image Quality, Applications*. 3rd ed. Erlangen: Publicis Publishing, 2011.

[16] Hounsfield GN. Computerized transverse axial scanning (tomography): Part I. Description of system. *Br J Radiol* 1973; 1016–102.

[17] Rubin GD. Computed tomography: Revolutionizing the practice of medicine for 40 years. *Radiology* 2014; 273: S45–S74.

[18] Buzug TM. *Computed Tomography: From Photon Statistics to Modern Cone-Beam CT*. Berlin, Heidelberg: Springer Berlin Heidelberg. Epub ahead of print 2008. DOI: 10.1007/978-3-540-39408-2.

[19] Kalender WA, Seissler W, Klotz E, et al. Spiral volumetric CT with single-breath-hold technique, continuous transport, and continuous scanner rotation. *Radiology* 1990; 176: 181–183.

[20] Ginat DT, Gupta R. Advances in Computed Tomography Imaging Technology. *Annu Rev Biomed Eng* 2014; 16: 431–453.

[21] European Comission. *Medical Radiation Exposure of the European Population: Radiation Protection N° 180*. Luxembourg, 2014.

[22] Wachabauer D, Stoppacher A, Mathis-Edenhof S. *Häufigkeiten medizinischer Anwendungen ionisierender Strahlung in Österreich*. Wien, 2015.

[23] NHS. *Diagnostic Imaging Dataset Annual Statistical*, http://www.wjgnet.com/1949-8470/full/v6/i1/1.htm (2017).

[24] Destatis. *Gesundheit: Fallpauschalenbezogene Krankenhausstatistik (DRG-Statistik) Operationen und Prozeduren der vollstationären Patientinnen und Patienten in Krankenhäusern (4-Steller)*. 2018.

[25] Seeram E. *Computed Tomography*. 4th Editio. Elsevier, 2015.

[26] Nowotny R, Sandborg M, Christofides S, et al. *Diagnostic Radiology Physics: A Handbook for Teachers and Students*. Vienna: International Atomic Energy Agency, 2014.

[27] Allisy-Roberts PJ, Williams J. *Farr's Physics for Medical Imaging: Second Edition*. 2007.

[28] Cheng Y, Abadi E, Smith TB, et al. Validation of algorithmic CT image quality metrics with preferences of radiologists. *Med Phys*. Epub ahead of print 2019. DOI: 10.1002/mp.13795.

[29] European Comission. European Guidelines on Quality Criteria for Computed Tomography European Guidelines on Quality Criteria. *Eur 16262 En* 1999; 1–71.

[30] Michael F. McNitt-Gray. Tradeoffs in CT Image Quality and Dose. *Med Phys*; 33.

[31] Silverman PM, Kalender WA, Hazle JD. Common terminology for single and multislice helical CT. *American Journal of Roentgenology*. Epub ahead of print 2001. DOI: 10.2214/ajr.176.5.1761135.

[32] Bushberg JT, Seibert JA, Leidholdt EM, et al. *The Essential Physics of Medical Imaging*. Third edit. Lippincott Williams & Wilkins, 2011. Epub ahead of print 2011. DOI: 10.1118/1.1585033.

[33] McNitt-Gray MF. AAPM/RSNA physics tutorialfor residents: Topics in CT: Radiation dose in CT. *Radiographics* 2002; 22: 1541–1553.

[34] Dendy PP, Heaton B. *Physics for diagnostic radiology: Third edition*. 2011. Epub ahead of print 2011. DOI: 10.1118/1.4795755.

[35] Bauhs JA, Vrieze TJ, Primak AN, et al. CT dosimetry: Comparison of measurement techniques and devices. *Radiographics* 2008; 28: 245–253.

[36] Shope TB, Gagne RM, Johnson GC. A method for describing the doses delivered by transmission x-ray computed tomography. *Med Phys*. Epub ahead of print 1981. DOI: 10.1118/1.594995.

[37] McCollough CH, Leng S, Yu L, et al. CT dose index and patient dose : They are not the same thing. *Radiology* 2011; 259: 311–316.

[38] Boone JM, Strauss KJ, Cody DD, et al. *Size-Specific Dose Estimates (SSDE) in Pediatric and Adult Body CT Examinations*. 2012.

[39] Fearon T, Vucich J. Normalized pediatric organ-absorbed doses from CT examinations. *Am J Roentgenol*. Epub ahead of print 1987. DOI: 10.2214/ajr.148.1.171.

[40] Bickers D, Lowy D. Carcinogenesis: A Fifty-Year Historical Perspective. *J Invest Dermatol* 1989; 92: S121–S131.

[41] Shah DJ, Sahcs RK, Wilson DJ. Radiation-induced cancer : a modern view. *Br J Radiol* 2012; 85: 1166–1173.

[42] Lall R, Ganapathy S, Yang M, et al. Low-dose radiation exposure induces a HIF-1-mediated adaptive and protective metabolic response. *Cell Death Differ* 2014; 21: 836–844.

[43] Siegel JA, Pennington CW, Sacks B, et al. The Birth of the Illegitimate Linear No-Threshold Model: An Invalid Paradigm for Estimating Risk Following Low-dose Radiation Exposure. *American Journal of Clinical Oncology: Cancer Clinical Trials*. Epub ahead of print 2018. DOI: 10.1097/COC.0000000000000244.

[44] Scott BR. Low-dose radiation risk extrapolation fallacy associated with the linear-no-threshold model. *Hum Exp Toxicol*. Epub ahead of print 2008. DOI: 10.1177/0960327107083410.

[45] Boice JD. The linear nonthreshold (LNT) model as used in radiation protection: An NCRP update. *International Journal of Radiation Biology*. Epub ahead of print 2017. DOI: 10.1080/09553002.2017.1328750.

[46] O ' Connor M, Murray PP, Foley SD, et al. *OPTIMISING COMPUTED TOMOGRAPHY OF OBESE PAEDIATRIC PATIENTS*. University College Dublin, 2017.

[47] Lambert JW, Phelps AS, Courtier JL, et al. Image quality and dose optimisation for infant CT using a paediatric phantom. *Eur Radiol* 2016; 26: 1387–1395.

[48] EASO. CHILDHOOD OBESITY (COTF). *The European Association for the Study of Obesity*, https://easo.org/about-easo/task-forces-groups/childhood-obesity/ (2016, accessed 20 November 2019).

[49] Armao D, Hartman T, Shea CM, et al. Developing a Toolkit for Pediatric CT Dose Reduction in Community Hospitals. *J Am Coll Radiol* 2016; 13: 1337–1342.

[50] Mathews JD, Forsythe A V., Brady Z, et al. Cancer risk in 680 000 people exposed to computed tomography scans in childhood or adolescence: Data linkage study of 11 million Australians. *BMJ* 2013; 346: 1–29.

[51] Krille L, Zeeb H, Jahnen A, et al. Computed tomographies and cancer risk in children: A literature overview of CT practices, risk estimations and an epidemiologic cohort study proposal. *Radiat Environ Biophys* 2012; 51: 103–111.

[52] De Gonzalez AB, Salotti JA, McHugh K, et al. Relationship between paediatric CT scans and subsequent risk of leukaemia and brain tumours: Assessment of the impact of underlying conditions. *Br J Cancer* 2016; 114: 388–394.

[53] Sun J, Peng Y, Duan X, et al. Image quality in children with low-radiation chest CT using adaptive statistical iterative reconstruction and model-based iterative

reconstruction. *PLoS One*; 9. Epub ahead of print 2014. DOI: 10.1371/journal.pone.0096045.

[54] American Association of Physicists in Medicine. *SPECIFICATION AND ACCEPTANCE TESTING OF COMPUTED TOMOGRAPHY SCANNERS*. New York, 1993.

[55] Chun M, Choi YH, Kim JH. Automated measurement of CT noise in patient images with a novel structure coherence feature. *Phys Med Biol* 2015; 60: 9107–9122.

[56] Lobo L, Antunes D. Chest CT in infants and children. *Eur J Radiol* 2013; 82: 1108–1117.

[57] Nagayama Y, Oda S, Nakaura T, et al. Radiation dose reduction at pediatric CT: Use of low tube voltage and iterative reconstruction. *Radiographics* 2018; 38: 1421–1440.

[58] Sun J, Hu D, Shen Y, et al. Improving image quality with model-based iterative reconstruction algorithm for chest CT in children with reduced contrast concentration. *Radiol Medica* 2019; 124: 595–601.

[59] Vorona GA, Zuccoli G, Sutcavage T, et al. The use of adaptive statistical iterative reconstruction in pediatric head CT: A feasibility study. *Am J Neuroradiol* 2013; 34: 205–211.

[60] Liu X, Chen L, Qi W, et al. Thin-slice brain CT with iterative model reconstruction algorithm for small lacunar lesions detection: Image quality and diagnostic accuracy evaluation. *Med (United States)*; 96. Epub ahead of print 2017. DOI: 10.1097/MD.0000000000009412.

[61] Gündoğdu S, Mahmutyazicioğlu K, Özdemir H, et al. Assessment of image quality of a standard and three dose-reducing protocols in adult cranial CT. *Eur Radiol* 2005; 15: 1959–1968.

[62] Young C, Xie C, Owens CM. Paediatric multi-detector row chest CT: What you really need to know. *Insights Imaging* 2012; 3: 229–246.

[63] Hyun Yang D, Woo Goo H. Pediatric 16-slice CT Protocols: Radiation Dose and Image Quality. *J Korean Radiol Soc* 2008; 59: 333.

[64] Phillips GS, Stanescu A-L, Alessio AM. Relationships of Pediatric Anthropometrics for CT Protocol Selection. *Am J Roentgenol* 2014; 203: W85–W91.

[65] Karmazyn B, Liang Y, Ai H, et al. Optimization of hybrid iterative reconstruction level in pediatric body CT. *Am J Roentgenol* 2014; 202: 426–431.

[66] Honnef D, Wildberger JE, Haras G, et al. Prospective evaluation of image quality

with use of a patient image gallery for dose reduction in pediatric 16-MDCT. *Am J Roentgenol* 2008; 190: 467–473.

[67] Waszczuk Ł, Guziński M, Garcarek J, et al. Triple-phase abdomen and pelvis computed tomography: Standard unenhanced phase can be replaced with reduced-dose scan. *Polish J Radiol* 2018; 83: e166–e170.

[68] Nievelstein RAJ, Van Dam IM, Van Der Molen AJ. Multidetector CT in children: Current concepts and dose reduction strategies. *Pediatr Radiol* 2010; 40: 1324–1344.

[69] Schuhbaeck A, Schaefer M, Marwan M, et al. Patient-specific predictors of image noise in coronary CT angiography. *J Cardiovasc Comput Tomogr* 2013; 7: 39–45.

[70] Kilic K, Erbas G, Guryildirim M, et al. Lowering the dose in head CT using adaptive statistical iterative reconstruction. *Am J Neuroradiol* 2011; 32: 1578–1582.

[71] Paolicchi F, Faggioni L, Bastiani L, et al. Optimizing the balance between radiation dose and image quality in pediatric head CT: Findings before and after intensive radiologic staff training. *Am J Roentgenol* 2014; 202: 1309–1315.

[72] Santos J, Foley S, Paulo G, et al. The impact of pediatric-specific dose modulation curves on radiation dose and image quality in head computed tomography. *Pediatr Radiol* 2015; 45: 1814–1822.

[73] Papadakis AE, Damilakis J. Automatic Tube Current Modulation and Tube Voltage Selection in Pediatric Computed Tomography: A Phantom Study on Radiation Dose and Image Quality. *Invest Radiol* 2019; 54: 265–272.

[74] Brisse HJ, Brenot J, Pierrat N, et al. The relevance of image quality indices for dose optimization in abdominal multi-detector row CT in children: Experimental assessment with pediatric phantoms. *Phys Med Biol* 2009; 54: 1871–1892.